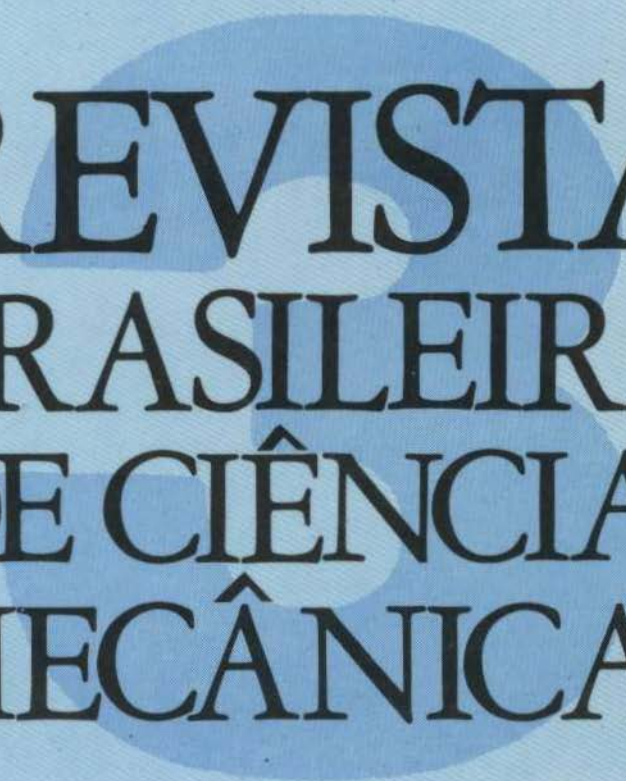


VOL. IX - N.º 3 - 1987

ISSN 0100-7386



REVISTA
BRASILEIRA
DE CIÊNCIAS
MECÂNICAS

PUBLICAÇÃO DA ABCM
ASSOCIAÇÃO BRASILEIRA DE CIÊNCIAS MECÂNICAS

A Revista Brasileira de Ciências Mecânicas é uma publicação técnico-científica, da Associação Brasileira de Ciências Mecânicas. Destina-se a divulgar trabalhos significativos de pesquisa científica e/ou tecnológica nas áreas de Engenharia Civil, Mecânica, Metalurgia, Naval, Nuclear e Química e também em Física e Matemática Aplicada. Pequenas comunicações que apresentem resultados interessantes obtidos de teorias e técnicas bem conhecidas serão publicadas sob o título de Notas Técnicas.

Os Trabalhos submetidos devem ser inéditos, isto é, não devem ter sido publicados anteriormente em periódicos de circulação nacional ou internacional. Excetuam-se em alguns casos publicações em anais e congressos. A apreciação do trabalho levará em conta a originalidade, a contribuição à ciência e/ou tecnologia, a clareza de exposição, a propriedade do tema e a apresentação. A aceitação final é da responsabilidade dos Editores e do Conselho Editorial.

Os artigos devem ser escritos em português, ou espanhol ou em inglês, datilografados, acompanhados dos desenhos em papel vegetal, em tamanho reduzido que permita ainda a redução para as dimensões da Revista e enviados para o Editor Executivo no endereço abaixo.

Editor Executivo da RBCM
Secretaria da ABCM
PUC/RJ - ITUC
Rua Marquês de São Vicente, 225 - Gávea
22453 - Rio de Janeiro, RJ - Brasil

A composição datilográfica será processada pela própria secretaria da RBCM de acordo com as normas existentes.

The Revista Brasileira de Ciências Mecânicas (Brazilian Journal of Mechanical Sciences) is a technical-scientific publication, sponsored by the Brazilian Association of Mechanical Sciences. It is intended as a vehicle for the publication of Civil, Mechanical, Metallurgical, Naval, Nuclear and Chemical Engineering as well as in the areas of Physics and Applied Mathematics. Short communications presenting interesting results obtained from well-known theories and techniques will be published under heading of the Technical Notes.

Manuscripts for submission must contain unpublished material, i.e., material that has not yet been published in any national or international journal. Exception can be made in some cases of papers published in annals or proceedings of conferences. The decision on acceptance of papers will take into consideration their originality, contribution to science and/or technology. The Editors and the Editorial Committee are responsible for the final approval.

The papers must be written in Portuguese, Spanish or English, typed and with graphics done on transparent white drawing paper in reduced size in such a way as to permit further reduction to the dimensions of the Journal, and sent to the Executive Editor at the following address.

Executive Editor of RBCM
Secretary of ABCM
PUC/RJ - ITUC
Rua Marquês de São Vicente, 225 - Gávea
22453 - Rio de Janeiro, RJ - Brazil

The final typing will be done by the secretary of RBCM according to the journal norms.



**EDITOR
RESPONSÁVEL**
Rubens Sampaio

**EDITOR
EXECUTIVO**
J. M. Freire

**CONSELHO
EDITORIAL**

Abimael F. D. Loula
Arthur J. V. Porto
Berend Snoeijer
Bernardo Horowitz
C. S. Barcellos
D. E. Zampieri
Duraíd Mahrus
E.O. Taroco Aliano
F. Venâncio Filho
F. E. Mourão Saboya
Giulio Massarani
Guillermo Creuss
Hans Ingo Weber
Henner A. Gomide
Jan Leon Scieszko
Jerzy T. Sielawa
J. J. Espíndola
Liu Hsu
Maurício N. Frota
Miguel H. Hirata
Nelson Back
Néstor Zouain
Nivaldo L. Cupini
O. Maizza Neto
Pedro Carajilescov
Sergio Colle

**A BOUNDARY ELEMENT ALGORITHM FOR
PLATE PROBLEMS**

157

J.A. Costa Jr. - Membro da ABCM
Departamento de Engenharia Mecânica - PUC/RJ

**THE STATE OF THE ART IN ADVANCED
HEAT-TRANSFER A REVIEW OF
TURBULENT BOUNDARY LAYER HEAT
TRANSFER**

173

Robert J. Moffat - Member of ABCM
Thermosciences Division
Department of Mechanical Engineering
Stanford University



A REVISTA BRASILEIRA DE CIÊNCIAS MECÂNICAS
É PUBLICADA COM O APOIO:

MCT – CNPq – FINEP

ANÚNCIOS NA RBCM

Qualquer solicitação de anúncios na revista deverá ser encaminhada
ao Representante exclusivo:

RIMTO COMUNICAÇÕES PUBLICITÁRIA LTDA.

Rio: Rua Conde de Bonfim, 370 Grs. 502/5/6/7/9

Tels.: 284-5842 (R) e 284-4920

SP: Rua Cel. Xavier de Toledo, 71 Grs. 602/3 – Tel.: 37-5252

DF: Shin QI 10 Cj. 7 – C/10 – Tel.: 577-2781

Formatos:

com margem 12,5 x 19,9 – sangrando 15,5 x 22,0

Todo o material deve ser fornecido pelo anunciante.

Fechamento: 30 dias antes do mês da circulação.

Circulação: Fevereiro – Maio – Agosto – Novembro.

Distribuição: Para todo o país.

Announcement and Call for Papers

FIRST WORLD CONFERENCE

ON

EXPERIMENTAL HEAT TRANSFER, FLUID MECHANICS AND THERMODYNAMICS

September 4-9, 1988 Dubrovnik, Yugoslavia

The objectives of the Conference are to bring together the experimental researchers and industrialists active in the areas of thermal and fluid science and engineering, to exchange their expertise and experiences in many research areas with cooperation and friendship, and to further stimulate their research activities. All participants will also have an opportunity to get informed on:

- advances in basic phenomena of heat transfer and fluid flow through conventional and sophisticated experiments
- state-of-the-art in experimental techniques and instrumentation
- innovative applications of research results through cross-fertilization of ideas from conference participants of various disciplines
- validity of experimental results in many fields
- definition of needs for further measurements
- experience gained and lessons learned from building test facilities and reducing test data

Papers dealing with experimental work together with theory, analysis and numerical studies on all aspects of heat transfer, fluid mechanics and thermodynamics will be considered. Also, papers analyzing original or existing experimental data together with theory or numerical results will be accepted.

The Conference Scientific Committee (made up of leading world authorities and experimentalists in heat transfer, fluid mechanics, and thermodynamics) is in charge of approving the acceptance of papers and final conference program.

Deadlines

- Nov. 1, 1987 Three copies of up to 1,000 word abstract.
- Dec. 1, 1987 Notify abstract acceptance
- Jan. 15, 1988 Full-length paper due
- Mar. 15, 1988 Notify paper acceptance
- Apr. 15, 1988 Author-prepared mats due

Send abstracts and further inquiry to: Professor Paulo Roberto de Souza Mendes, Department of Mechanical Engineering, Pontifícia Universidade Católica do Rio de Janeiro, Rua Marquês de São Vicente, 225, CEP 22453, Rio de Janeiro, RJ, BRASIL.

A BOUNDARY ELEMENT ALGORITHM FOR PLATE PROBLEMS

J. A. Costa Jr. - Membro da ABCM
PUC/RJ - Departamento de Engenharia Mecânica

ABSTRACT

In this paper the Boundary Element Method is used to analyse plate problems such as: plate bending, plate on elastic foundations, buckling and vibration of plates. The direct method is used to obtain the integral formulation of the various problems in a general form. The computer algorithm developed to implement the formulation is capable of solving a variety of physical problems. Some examples are presented to illustrate the applicability of the algorithm.

RESUMO

Neste trabalho o Método dos Elementos de Contorno é usado para analisar problemas de placas tais como: flexão simples, flexão sobre fundação elástica, flambagem e vibração de placas. O método direto é usado para obter a formulação integral dos vários problemas em uma forma geral. O algoritmo desenvolvido para implementar a formulação, é capaz de resolver uma variedade de problemas físicos. Vários exemplos são apresentados para ilustrar a sua aplicabilidade.

INTRODUCTION

The Boundary Element Method has recently become a powerful technique for solving different types of engineering problems. Its main advantage is that it reduces the dimensionality of a given problem.

Recent developments of the method for plate problems employing the direct method are described in references [1,2,4,5,6,7,9,12,19].

In this paper, separate formulations [4,5,7,9] proposed by the present author are presented together in an integrated form. The general form, which is described briefly here, is part of a computer algorithm developed to solve various plate problems numerically. Numerical examples for a number of plate problems are obtained by the code and the results are presented here. They are compared with analytical and numerical solutions obtained independently by other authors.

PRELIMINARY CONSIDERATIONS AND BASIC EQUATIONS

The governing differential equations of plate problems developed in accordance with the classical thin plate theory, are defined as follows.

Plate Bending

The differential equation for a plate of constant thickness and subjected to a distributed load $q(X_1, X_2)$ is

$$D \nabla^4 w = q \quad \text{for } w \text{ in } \Omega \quad (1)$$

where ∇^4 denotes the biharmonic operator in cartesian coordinates X_1 and X_2 , w is the displacement in the domain Ω bounded by the curve Γ .

$D = Eh^3/12(1-\nu^2)$ is the flexural rigidity, E and ν are Young's Modulus and Poisson's Ratio respectively, and h is the plate thickness.

Plate Bending on Elastic Foundations

In the case of plates on elastic foundations, the load distribution of $q(X_1, X_2)$ in equation (1) is assumed to be divided into two parts:

$$\text{i.e.} \quad q = q_1 + q_2 \quad (2)$$

q_1 is a given external load acting on the plate and q_2 is the

reaction of the foundation due to the deflection of the plate. It is possible to assume the following relationship (Winkler's Foundation)

$$q_2 = -K w \quad (3)$$

where K is the foundation modulus. Substituting equation (3) into equation (1), the differential equation (1) assumes the form

$$\nabla^4 w + \lambda_e^4 w = \frac{q}{D} \quad (4)$$

where λ_e is the parameter defined as $\lambda_e^4 = K/D$.

Vibration

The governing differential equation for the free vibration of a homogeneous isotropic, linear elastic plate of uniform thickness is

$$D \nabla^4 w + \rho \frac{\partial^2 w}{\partial \hat{t}^2} = 0 \quad \text{for } w \text{ in } \Omega \quad (5)$$

where ρ is the mass per unit area and t is the time.

Assuming a harmonic vibration, it is possible to write

$$w(X_1, X_2, \hat{t}) = w(X_1, X_2) \sin \omega \hat{t} \quad (6)$$

where ω is the natural frequency of the plate.

Substituting equation (6) into equation (5) gives

$$\nabla^4 w - \lambda_v^4 w = 0 \quad \text{for } w \text{ in } \Omega \quad (7)$$

where λ_v is the frequency parameter defined as $\lambda_v^4 = \omega^2 \rho/D$.

Buckling

The governing differential equation for the buckling of an elastic plate subjected to the action of in-plane boundary forces N_{X_1} , N_{X_2} and $N_{X_{1,2}}$ is

$$D \nabla^4 w - P_C \sum_{i,j=1}^2 \left[N_{X_{i,j}} \frac{\partial^2 w}{\partial X_i \partial X_j} \right] = 0 \quad (8)$$

where P_C is a multiplying factor for the buckling load.

FUNDAMENTAL SOLUTIONS

The basic fundamental solutions for plate problems should satisfy the following differential equations[3]

$$L(u) = \delta(X_1 - \bar{X}_1, X_2 - \bar{X}_2) / D \quad (9)$$

and

$$L(u) = - \frac{\partial}{\partial n_0} \delta(X_1 - \bar{X}_1, X_2 - \bar{X}_2) / D \quad (10)$$

where L is the differential equation governing the plate problems, \bar{X}_1, \bar{X}_2 are the coordinates of the internal point and $\delta(X_1, X_2)$ is the two-dimensional Dirac Delta function $\delta(X_1) \delta(X_2)$ which is written as $\delta(X_1, X_2)$ for conciseness. In equation (10), \bar{n}_0 represents an arbitrary but known direction.

The Fourier technique can be used to solve equation (9) which represents the fundamental solution obtained when a unit concentrated force is applied at an internal point within a plate.

From the theory of generalized functions, it is known that if u is a solution of $Lu = \delta$ (where L is a differential operator with constant coefficients), its derivative $\partial u / \partial \alpha$ is a solution of $Lu = \partial \delta / \partial \alpha$ [10]. Consequently, from this and the solution of equation (9) it is possible to obtain the fundamental solution of equation (10).

The generalised delta function δ has derivatives of all orders [13], and consequently it is possible to define another solution which satisfies the following equation

$$L(u) = \frac{\partial^2}{\partial x_m \partial x_k} (\delta(X_1 - \bar{X}_1), (X_2, \bar{X}_2)) / D \quad \text{for } m, k = 1, 2 \quad (11)$$

The same considerations used to obtain the solution of equation (10) can be employed to find the solution of equation (11). The solutions of the previously mentioned equations for various differential operators related to plate problems are provided within Appendix 1.

INTEGRAL EQUATIONS

The plate equations (1), (4), (7) and (8) with their respective fundamental solutions which are provided within Appendix 1, can now be reduced to integral equations.

Multiplying these equations and their associated fundamental solutions by u_p ($\alpha = 0, 1, 2$, and $p = 1, 2, 3, \dots, 5, 6$) and w respectively, and then subsequently subtracting and integrating over the domain Ω , yields

$$D \int_{\Omega} (u_p^\alpha \nabla^4 w - w \nabla^4 u_p^\alpha) d\Omega - J^\alpha = \int_{\Omega} (-1)^\alpha f^\alpha(\delta(\cdot)) d\Omega$$

for $\alpha = 0, 1, 2$ and $p = 1, 2, 3, 4, 5, 6$ (12)*

where,

$$f^0(\cdot) = 1, \quad f^1(\cdot) = \frac{\partial}{\partial n_0}(\cdot) \quad \text{and} \quad f^2(\cdot) = \frac{\partial^2}{\partial x_m \partial x_k}(\cdot)$$

and

$$J^\alpha \text{ are equal to } \begin{cases} \int_{\Omega} q u_p^\alpha d\Omega, & \text{for } p = 1, 2 \\ 0, & \text{for } p = 3, 4 \\ \int_{\Omega} w \lambda_v^\alpha u_p^\alpha d\Omega, & \text{for } p = 5 \\ \int_{\Omega} \sum_{i,j=1}^2 [N_{X_{i,j}} \frac{\partial^2 w}{\partial X_i \partial X_j}] u_p^\alpha d\Omega, & \text{for } p = 6 \end{cases}$$

The equations provided above (12), can be reduced to another type of integrals by using the Rayleigh Green identity, which for a region with M corners [1,5,15] gives,

$$D \int_{\Omega} (v \nabla^4 w - w \nabla^4 v) d\Omega = \int_{\Gamma} \left[V_n(v)w - M_n(v) \frac{\partial w}{\partial n} + \frac{\partial v}{\partial n} M_n(w) - v V_n(w) \right] d\Gamma - \sum_{m=1}^M \left(w \Big|_{-}^{+} M_t(v) - v \Big(\Big|_{-}^{+} M_t(w) \right) \right) \quad (13)$$

* Note: Formula (12) represents three separate equations ($\alpha = 0, 1, 2$) which are needed for each plate problem p .

where at a regular point,

$$M_n(w) = -D \left| -\nabla^2 w + (1-\nu) \sum_{J,L=1}^2 \cos(\bar{n}, \bar{x}_J) \cos(\bar{n}, \bar{x}_L) \frac{\partial^2 w}{\partial x_J \partial x_L} \right.$$

$$M_t(w) = D \left| -(1-\nu) \sum_{J,L=1}^2 (-1)^L \cos(\bar{n}, \bar{x}_J) \cos(\bar{n}, \bar{x}_{3-L}) \frac{\partial^2 w}{\partial x_J \partial x_L} \right.$$

$$V_n(w) = -D \frac{\partial}{\partial n} \nabla^4 w + \frac{\partial}{\partial t} M_t(w) . \quad (14)$$

\bar{n} and \bar{t} represent the normal and tangent to the boundary respectively, ν is a function with a sufficient degree of continuity.

The definition of $|_{-}^{+}$ at a point s is:

$$|_{-}^{+} M_t(s) = M_t(s+0) - M_t(s-0) \quad (15)$$

Hence, using relation (13) to express the first term in equation (12) and consequently estimating some of its results under the condition of a point on a smooth boundary, it is possible to obtain the following:

$$cf^\alpha(w(\xi)) = J^\alpha - \int_{\Gamma} \left[V_n(u_p^\alpha(\xi, \theta)) [w(\theta) - \beta w(\xi)] \right.$$

$$- M_n(u_p^\alpha(\xi, \theta)) \frac{\partial w}{\partial n} + \frac{\partial}{\partial n} (u_p^\alpha(\xi, \theta)) M_n(\theta)$$

$$- u_p^\alpha(\xi, \theta) V_n(\theta) \left. \right] d\Gamma + \sum_{m=1}^M [w(\theta) - \beta w(\xi)] (|_{-}^{+} M_t(u_p^\alpha(\xi, \theta)))$$

$$- u_p^\alpha(\xi, \theta) (|_{-}^{+} M_t(\theta))$$

$$\text{for } \alpha = 0, 1, 2 \text{ and } p = 1, 2, 3, \dots, 6 \quad (16)**$$

where c and β are equal to $\left\{ \begin{array}{ll} c = 1, & \beta = 0, \quad \xi \in \Omega \\ c = 1/2, & \beta = 1, \quad \xi \in \Gamma \\ c = 1, & \beta = 0 \end{array} \right. \quad \text{for } \alpha = 0, 1$
 $\left. \begin{array}{ll} & \\ & \\ c = 1, & \beta = 0 \end{array} \right\} \quad \text{for } \alpha = 2 ;$

** Note: Subscripts and superscripts appearing more than once designate variables in the respective equations.

and $\xi = (X_1, X_2)$, $\theta = (\bar{X}_1, \bar{X}_2)$ in equations (16) represent the source and field points respectively.

Finally, when $p = 1, 2$ the domain integrals J of equation (16) can be transferred to the boundary in order to preserve the reduced dimensionality characteristics of the Boundary Element Method [4,8].

NUMERICAL IMPLEMENTATION

The integral equation (16), can be reduced to a system of algebraic equations by discretizing the boundary and domain (if it is required) using boundary element and internal cells, respectively. Following the procedure employed previously in [5,7], the boundary can be approximated by N boundary constant elements and the domain by M cells. The integrals can be performed using Gaussian quadrature formulae for the case of a non-singular integral and a combination of semi-analytical and analytical for the singular situation. Moreover, the twist moment $M_t(\theta)$ can be expressed in terms of the normal slope $\partial w / \partial n$ [5]. After which, it is possible to express the algebraic equations as described within the following matrices

$$\begin{bmatrix} H_p^{11} & H_p^{12} \\ H_p^{21} & H_p^{22} \\ \text{-----} \\ H_p^{l1} & H_p^{l2} \end{bmatrix} \begin{bmatrix} w \\ \frac{\partial w}{\partial n} \end{bmatrix} = \begin{bmatrix} G_p^{11} & G_p^{12} \\ G_p^{21} & G_p^{22} \\ \text{-----} \\ G_p^{l1} & G_p^{l2} \end{bmatrix} \begin{bmatrix} V_n \\ M_n \end{bmatrix} + \begin{bmatrix} B_p^1 \\ B_p^2 \\ \text{---} \\ B_p^l \end{bmatrix} \begin{bmatrix} D_p^1 \\ D_p^2 \\ \text{---} \\ D_p^l \end{bmatrix} \quad (17)$$

The subscripts $p(1,2,3,4,5,6)$ indicate that the problem is being treated by the algebraic form of equations (16), from which the matrices are assembled. $[H]$ is a $(2N+iM) \times 2N$ matrix whose coefficients originate from the integrals and corner contributions related to the displacement and normal slope (densities) of the algebraic equations created by the discretization of equations (16). $[G]$ is a $(2N+iM) \times 2N$ matrix whose coefficients develop from the integrals related to the shear force and moment densities of the algebraic equations resulting from the discretization of equations (16). $[B]$ is a $(2N+iM) \times iM$ matrix whose coefficients result from the domain integrals and the internal densities after discretization

of equations (16). $[D]$ is a $iM \times 1$ column vector of the internal densities and results from the discretization of equations (16).

were: $l = 0, i = 0$ for $p = 1, 2, 3, 4$
 $l = 3, i = 1$ for $p = 5$
 $l = 5, i = 3$ for $p = 6$

At a regular point on the boundary the known densities $(w, \partial w / \partial n, M_n(w), V_n(w))$ are:

Clamped boundary: w and $\frac{\partial w}{\partial n}$,

Simply supported boundary: w and M_n ,

Free boundary: V_n and M_n ,

Mixed boundary: combination of the above three.

Taking into account the boundary conditions outlined above, it is possible to express the system (17) for each particular plate problem as follows:

Plate Bending $p = 1, 2$

$$[A_p]_{\Gamma\Gamma} \{\bar{X}\} = [B_p]_{\Gamma\Gamma} \quad (18)$$

and

$$\{\bar{Y}\} = [A_p]_{\Omega\Gamma} \{\bar{X}\} + [B_p]_{\Omega\Gamma} \quad (19)$$

Vibration and Buckling

For the case $p = 3, 4$

$$[A_p]_{\Gamma\Gamma} \{\bar{X}\} = 0 \quad (20)$$

and for $p = 5, 6$

$$\left[[A_p]_{\Omega\Gamma} [A_p]_{\Gamma\Gamma}^{-1} [B_p]_{\Omega\Gamma} - [B_p]_{\Omega\Omega} \right] \{\bar{Y}\} = \frac{1}{\lambda_p} \{\bar{Y}\} \quad (21)$$

where λ_p are the eigenvalues for the referred plate problem p , $\{\bar{X}\}$

is the column vector of the unknown boundary densities and $\{\tilde{Y}\}$ represents the vector of the unknown densities.

Finally, a boundary element computer program for analysing the problems discussed within this paper has been developed. The computer code for the algorithm is written in conversational mode capable of accommodating plates with various loading and boundary conditions. The flow chart, which expresses the logic of the computer program coded in FORTRAN, is presented in Appendix 2.

EXAMPLES

Example 1

This example consists of a circular plate with clamped edges subjected to a uniformly distributed load. The cases studied here are: plate bending and plate on elastic foundation. The following data were used:

Radius of plate = $a = 10$ in

Uniform pressure load = $q = 1000$ psi

Flexural rigidity of plate = $D = 10^6$ in.lb

Modulus of foundation = $K = 0$, and $K = 2 \times 10^4$ lb/in³

Poisson's ratio = 0.30

Results for the centre deflection and bending moments computed by BEM using constant boundary discretizations are presented in Table 1. These results are compared against analytical solutions obtained by NG reference [14].

It is apparent from Table 1 that the BEM results agree closely with those of NG [14]. It is also interesting to point out that the accuracy of these results is obtained using small number of boundary elements. It is interesting to point out that the BEM results for the centre moment is slight greater than the analytical solution for $K = 0$. It is felt that more elegant numerical techniques would eliminate this minor problem.

Example 2

This example studies the buckling and vibration of a square plate with two opposite sides simply supported and the other two edges clamped. For the buckling case, the inplane loading considered is $N_{X_{1,2}}$ constant and $N_{X_1} = N_{X_2} = 0$. The eigenvalues are given by

$$\text{Natural vibration: } \lambda_v = w / \sqrt{D/\rho L^4}$$

$$\text{Buckling: } \lambda_b = N_{X_{1,2}} L^2 / \pi^2 D$$

where L is the side length of the square plate.

Table 1. Comparison of maximum deflection, maximum centre moment and edge moments

Coefficient w for maximum deflection at centre

$$w_{\text{MAX}} = \frac{w a q}{D} (10^{-2})$$

Moment coefficient c and m

$$\text{Centre moment } M_R = c q a^2 (10^{-2})$$

$$\text{Edge moments } M_R = -m q a^2 (10^{-2})$$

Foundation Modulus K · lb/in ³	Deflection		Centre Moment		Edge Moments	
	BEM	Ref. NG[14]	BEM	Ref. NG[14]	BEM	Ref. NG[14]
0	1.5125* 1.5386** 1.5479***	1.5625	8.025 8.169 8.220	8.125	12.10 12.31 12.39	12.500
2 × 10 ⁴	0.4876* 0.4936** 0.4957***	0.4980	2.049 2.006 1.990	1.972	5.99 5.83 5.76	5.694

Legend:

*, **, *** : These results were obtained using 16, 24 and 32 total number of boundary elements respectively.

The results obtained by BEM using different discretization for the domain and boundary are presented in Table 2. It can be seen from Table 2 that the results agree well with analytical solutions. It is also interesting to point out that the BEM results for buckling and vibration (higher modes) are in better agreement with the analytical solution (Table 2) than those obtained using FEM, for the specific finite elements described in references [17,16].

Table 2. Comparison of buckling and vibration eigenvalues of a square plate with two opposite sides simply supported and the other two edges clamped

NATURAL VIBRATION CASE					
Eigenvalues λ_v	BEM SOLUTIONS			Exact [16]	FEM [16]
	BE \times CELLS				
	16 \times 24	16 \times 32	28 \times 50		
λ_1	30.6	30.3	30.0	29.0	28.1
λ_2	58.1	57.5	57.0	54.8	51.5
λ_3	79.6	73.0	71.8	69.3	64.25
BUCKLING CASE, LOADING $N_{X_{1,2}}$ CONSTANT					
Eigenvalues λ_b	BEM SOLUTIONS			Exact [17]	FEM [17]
	BE \times CELLS				
	16 \times 24	16 \times 32	28 \times 50		
λ_1	12.97	12.77	12.56	12.28	13.370

CONCLUSIONS

A powerful computer boundary element code has been developed to analyse different plate problems. The results have been compared against analytical solutions for a variety of plate problems with different geometries, loading and boundary conditions. The tests show that the algorithm is capable of providing accurate results. The interactive version of the code developed for the research will now be optimized and adapted to have graphic facilities. The present algorithm automatically generates the boundary elements and internal mesh required to run the plate problem.

ACKNOWLEDGEMENTS

The author is indebted to the CNPq (National Council for Scientific and Technological Development - Brazil) for their support of this work.

REFERENCES

- [1] Bezzine, G., Boundary integral formulation for plate flexure

- with arbitrary boundary conditions. Mech. Res. Comm., 5 pp.197-206 (1978).
- [2] Bezine, G., A mixed boundary integral - Finite element approach to plate vibration problems. Mech. Res. Comm., 7 : pp.141-150 (1980).
- [3] Chernyshev, G.N., On the action of concentrated forces and moments on an elastic thin shell of arbitrary shape. Journal of Applied Mathematics and Mechanics, 27 : pp.271-284 (1963).
- [4] Costa Jr., J.A. and Brebbia, C.A., Plate bending problems using BEM. VI International Conference of Boundary Element Methods, Springer-Verlag, p.343-363 (1984).
- [5] Costa Jr., J.A. and Brebbia, C.A., The boundary element method applied to plates on elastic foundations. Journal Engineering Analysis, 2 (4) : 174-183 (1985).
- [6] Costa Jr., J.A. and Brebbia, C.A., Bending of plates on elastic foundations using the boundary element method. II International Conference on Variational Methods in Engineering, Southampton, UK, 1985. Springer-Verlag, Berlin & NY (1985).
- [7] Costa Jr., J.A. and Brebbia, C.A., Elastic buckling of plates using boundary element methods. VII International Conference on Boundary Element Methods in Engineering, Lake Como, Italy 1985. Springer-Verlag, Berlin & NY (1985).
- [8] Costa Jr., J.A. and Brebbia, C.A., On the reduction of domain integrals to the boundary for the BEM formulation of plates on elastic foundation. Engineering Analysis, 3 (3) : 123-126 (1986).
- [9] Costa Jr., J.A., Plate vibrations using BEM. Applied Mathematical Modelling, to appear.
- [10] Gel'Fand, I.M. and Shilov, G.E., Generalized functions. vol.1, Academic Press Inc., New York (1967).
- [11] Katsikadelis, J.T. and Armenakas, A.E., Plates on elastic foundation by BIE method. Journal of the Structural Division ASCE, 110 : 1086-1105 (1984).
- [12] Katsikadelis, J.T. and Armenakas, A.E., Analysis of clamped plates on an elastic foundation by the boundary integral method. Journal of Applied Mechanics, 54 : 544-580 (1984).
- [13] Lighthill, M.J., Fourier analysis and generalized functions. Cambridge University Press (1958).

- [14] NG, S.S.F., Influence of elastic support on the behaviour of clamped plates. Developments in Mechanics, 5. Proc. 11th Midwestern Mechanics Conference, pp.353-371 (1969).
- [15] Stern, M., A general boundary integral formulation for the numerical solution of plate bending problems. Int. J. Solids Structures, 15 : 769-782 (1972).
- [16] Szilard, R., Theory and analysis of plates. Prentice Hall, (1974).
- [17] Tabarrok, B.; Fenton, R.G. and Elsaie, A.M., Application of a refined plate bending element to buckling problems. Computers & Structures, 4 : 1313-1321 (1974).
- [18] Timoshenko, S.P. and Gere, J.M., Theory of elastic stability. McGraw-Hill, NY (1961).
- [19] Wong, G.I.K. and Hutchinson, J.R., An improved boundary element method for plate vibrations. Proceedings of the Third International Seminar on Boundary Element Methods, Irvine, California, July 1981. Springer-Verlag, Berlin & NY (1981).

APPENDIX I - FUNDAMENTAL SOLUTIONS

Plate Problems	Operator L	Solution of eqs. (9), (10) and (11) respectively
P=1 Plate bending		$u_P^0 = \frac{r^2 (\ln r - 0.5)}{8\pi D}$
P=5 Vibration* and	$L = \nabla^4$	$u_P^1 = - \frac{\partial}{\partial n_0} (u_P^0)$
P=6 Buckling		$u_P^2 = \frac{\partial}{\partial X_m \partial X_k} (u_P^0)$
P=2 Plates on elastic foundations	$L = \nabla^4 + \lambda_e$	$u_P^0 = - \frac{1}{2\pi\lambda_e^2} \text{Kei}(\lambda_e r)$ $u_P^1 = - \frac{\partial}{\partial n_0} (u_P^0)$ $u_P^2 = \frac{\partial}{\partial X_m \partial X_k} (u_P^0)$
P=3 Vibration of plates	$L = \nabla^4 - \lambda_v$	$u_P^0 = - \frac{i}{8\pi\lambda_v^2} [H_0(\lambda_v r) - H_0(i\lambda_v r)]$ $u_P^1 = - \frac{\partial}{\partial n_0} (u_P^0)$
P=4 Buckling of plates	$L = \nabla^4 + \lambda_b \nabla^2$	$u_P^0 = \frac{1}{4\lambda_b^2} [K_0(\lambda_b r) - \frac{2}{\pi} \ln r]$ $u_P^1 = - \frac{\partial}{\partial n_0} (u_P^0)$

where,

Kei is a Kelvin function of zero order

$H_0(z)$ is the Hankel function of the first kind

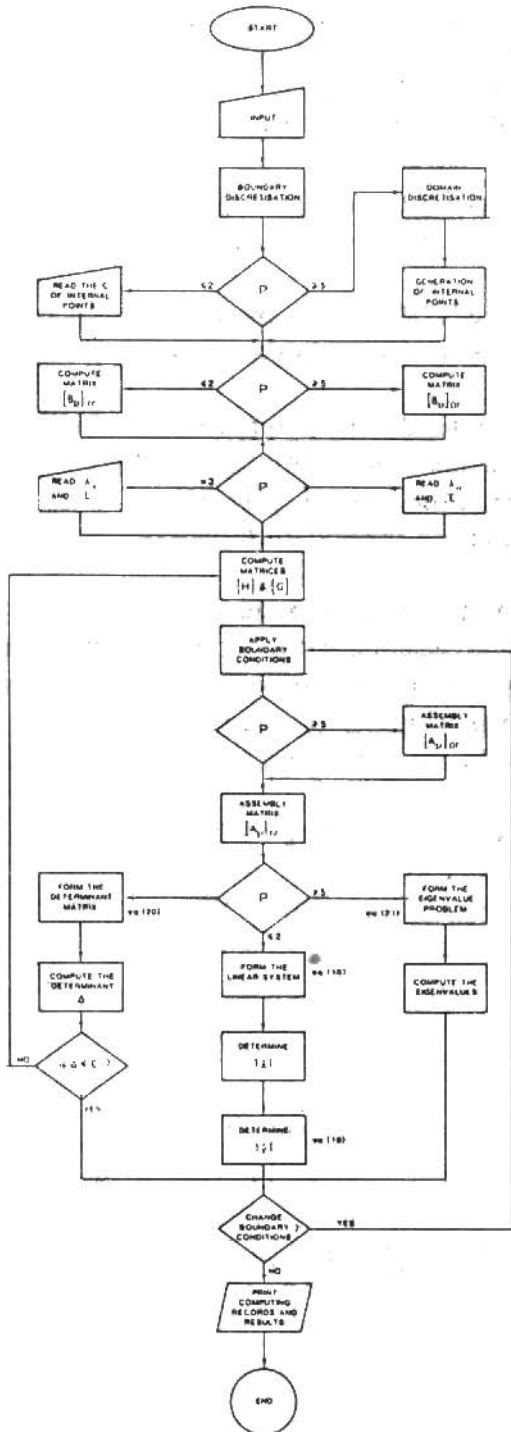
$K_0(z)$ is the modified Bessel function of the second kind

$\lambda_b^2 = N/D$, $N = N_{X_1} = N_{X_2}$ and $N_{X_{1,2}} = 0$

* Vibration and Buckling formulations using the static fundamental solution of plate bending

$$r^2 = (X_1 - \bar{X}_1)^2 + (X_2 - \bar{X}_2)^2$$

APPENDIX II
 FLOW CHART OF THE
 GENERAL PROGRAM



THE STATE OF THE ART IN ADVANCED HEAT-TRANSFER A REVIEW OF TURBULENT BOUNDARY LAYER HEAT TRANSFER

Robert J. Moffat - Member of ABCM
Thermosciences Division
Department of Mechanical Engineering
Stanford University

The development of the aircraft gas turbine, over the past 35 years, has stimulated considerable research in turbulent boundary layer heat transfer. The high-temperature gas turbine poses many challenging heat transfer problems of a boundary layer nature. Vanes, blades, combustion chamber liners, and some interior gas passages are exposed to gases at the maximum cycle temperature of the engine. As engine temperatures rose in the quest for higher efficiency and power density, the problem of protecting the surfaces from thermal damage became more difficult to solve. Thermal protection can be achieved by any of several approaches or combinations of approaches: insulating coatings, such as ceramics; internal cooling with liquid metals, pressurized water or boiling water; internal cooling with gases (air or steam); or boundary layer thermal control (transpiration, slot cooling, or discrete-hole injection); full- or partial-coverage. Whichever system is used, the temperature level and heat load are affected by the behavior of the boundary layer on the surface. Understanding the factors which affect boundary layer heat transfer is crucial to any thermal design. Two different types of heat transfer calculations need to be done: design surveys and detailed analyses. These require different analytical methods and different types of data to support the methods. In both types of analysis, the target accuracy is high, at the moment beyond the state of the heat transfer art. To illustrate, in highly stressed components, such as turbine blades, a difference of 25°F (14°C) can mean a factor of two in blade life. This may correspond to a change of less than 5% in the value of the boundary layer heat transfer. The current state of the art does not allow calculations of that accuracy, except under laboratory conditions. The heat transfer coefficients on engine structures have sometimes been found to be as much as 50% different from the calculated values, even using the best current methods. Designers have been forced to use large safety factors on cooling flows, with the attendant penalties on engine performance.

This situation has led to continual efforts to improve the accuracy of predictions, supported by extensive, practical, and careful research.

In the sections which follow, data will be presented which illustrate the effects of several environmental parameters known to affect heat transfer. Then some comments will be made concerning calculation procedures and some physically based models presented which have been successful in calculating heat transfer rates.

Most, but not all, of the data presented here came from heat transfer research in the Thermosciences Division of Stanford University. This research program began in 1958 and has been in continuous operation since then. Twenty-two doctoral programs were completed during this period, involving five different research wind tunnels -- all related to an organized study of boundary layer heat transfer.

The preponderance of Stanford data does not reflect any disregard for the significant contributions by other groups. In many cases, our programs were started because of publication of a new result or a new theory from some other group.

THE GOVERNING EQUATIONS

It will be convenient to sort the environmental effects into categories and to discuss their effects in terms of the governing differential and integral equations of the boundary layer.

Let us consider the baseline problem to be fully developed turbulent flow along a smooth plate of uniform temperature and then look at the effects of other factors. At least ten factors are presently recognized which may alter the heat transfer coefficient from the baseline values: variable wall temperature, acceleration of the main stream, deceleration, free stream turbulence, surface roughness, transpiration through the surface, injection through slots or holes, curvature of the surface, unsteadiness in the main-flow velocity or direction, and secondary flows. The data which follow will illustrate the first eight of these effects.

Each data set to be shown consists of Stanton number versus x-Reynolds number (or enthalpy thickness Reynolds number) and shows the main effect of the parameter being studied. For purposes of prediction, however, such results are not enough. In the original research works, velocity and temperature distributions and turbulence quantities generally were measured, and from each data set information has been extracted about the turbulent transport of heat and momentum which was then incorporated into a two-dimensional boundary layer predictor program. The Prandtl mixing-length model is one of the closure methods used for calculating the distribution of mean velocity. A turbulent Prandtl number function is used for calculating the temperature distribution. One widely used program, STAN5, was described by Crawford and Kays (1976). Turbulence kinetic energy closures are also used. All such programs depend on data as sources for their modeling constants.

The differential equations for conservation of x-momentum and mass in a constant-properties, turbulent flow are shown below, to illustrate the way in which the experimental data are used:

$$U \frac{\partial U}{\partial X} + v \frac{\partial U}{\partial Y} - \frac{\partial}{\partial y} (\epsilon_M + v) \frac{\partial U}{\partial Y} = - g_c \frac{dp}{dX} \quad (1)$$

$$\frac{\partial U}{\partial X} + \frac{\partial v}{\partial Y} = 0 \quad (2)$$

These equations can be solved if the coefficients and boundary conditions are provided: ϵ_M , v , $\frac{dp}{dX}$, $U(X,0)$, $U(X,\Delta)$, $U(0,y)$. The principal experimental input is in ϵ_M , the eddy diffusivity. The Prandtl mixing length model gives:

$$\epsilon_M = \ell^2 \left| \frac{\partial U}{\partial Y} \right| \quad (3)$$

where

$$\ell = 0.41 Y [1 - \exp\{-Y^+/A^+\}] \quad (4)$$

The mixing-length region can be thought of as two sub-regions: a damped mixing-length region, very near the wall, and an undamped outer region. There is ample evidence that the outer-region mixing length is relatively universal: most of the variation in mixing length occurs very near the wall. In the work at Stanford, the damping parameter A^+ , introduced by van Driest, is used as a variable, affected by transpiration, pressure gradient, roughness,

and curvature. This has allowed successful prediction of most of the cases studied to date

The energy equation for a constant-properties flow along a flat surface with no chemical reaction is:

$$U \frac{\partial T}{\partial X} + v \frac{\partial T}{\partial Y} - \frac{\partial}{\partial Y} (\epsilon_H + \alpha) \frac{\partial T}{\partial Y} = 0 \quad (5)$$

The principal experimental input is in the eddy diffusivity for heat, ϵ_H . This information can be approached via the turbulent Prandtl number:

$$\epsilon_H \stackrel{\Delta}{=} \frac{\epsilon_M}{Pr_T} \quad (6)$$

where the experimental task is to measure Pr_T within the boundary layer under the influence of the various parameters.

The general approach, at Stanford, has been to use data from equilibrium boundary layer studies for developing the models for A^+ and Pr_T and to check the predictions against data from non-equilibrium situations, as a test of the generality of the prediction.

When one wishes to test variable velocity or variable transpiration, one needs a scalar parameter related to "strength of acceleration" (or deceleration) or "strength of blowing." The momentum integral equation provides guidance, as seen below. Eqn. (7) is the 2-D momentum integral equation for constant-density flow along a flat surface:

$$\frac{C_f}{2} + \frac{\dot{m}''}{G} = \frac{C_{f0}}{2} (1 + B_f) = \frac{d\delta_2}{dX} + \delta_2 \left[(2 + H) \frac{1}{U_\infty} \frac{dU_\infty}{dX} \right] \quad (7)$$

The blowing parameter B_f appears naturally in Eqn. (7).

$$B_f \stackrel{\Delta}{=} \frac{\dot{m}''}{G(C_{f0}/2)} \quad (8)$$

Equation (7) can be rearranged to show

$$\frac{d}{dX} (U_\infty^2 \delta_2) = \frac{g_c \tau_o}{\rho_\infty} \left[1 + G(C_{f0}/2) + \frac{\delta_1}{\tau_o} \frac{dp}{dx} \right] \quad (9)$$

A new parameter appears, $\beta = (\delta_1/\tau_0)(dp/dX)$, which can be held constant by properly adjusting the pressure gradient as the boundary layer thickness grows.

A different rearrangement is:

$$\frac{d\text{Re}\delta_2}{(U_\infty dX/\nu)} = \frac{C_f}{2} + \frac{\dot{m}''}{G} - \frac{\nu}{U_\infty^2} \frac{dU_\infty}{dX} (1 + H) \text{Re}\delta_2 \quad (10)$$

In Eqn. (10), if the acceleration parameter $K = (\nu/U_\infty^2)(dU_\infty/dX)$ is held constant, the boundary layer will reach an equilibrium state where $d\text{Re}\delta_2/(U_\infty dX/\nu) = 0$.

The data for accelerating flows data shown in this collection were taken with constant K . For decelerating flows, the value of β was held constant. This was done by making the free stream velocity vary as:

$$U_\infty = CX^m \quad (m < 0) \quad (11)$$

Transpiration data will be presented mainly in terms of constant blowing fraction, $F = \dot{m}''/G$. While constant F does not result in an equilibrium state, it has been verified experimentally that constant F and constant B flows produce equivalent results when interpreted in terms of local state descriptors; the path of approach to the state is of secondary importance.

EXPERIMENTAL APPARATUS

Five different research tunnels have been used in the course of the research reported here, covering the 25 years from 1958 (Reynolds et al., 1958a) to Furuhashi, 1983. Reynolds' early work was done on a sharp-edged flat plate suspended on the centerline of a large, open-throat wind tunnel. The test plate was about 0.5 meter wide and 1.5 meter long, instrumented with heat flux meters and surface temperature thermocouples. The plate was electrically heated and the resulting heat flux measured using imbedded heat-flux transducers.

Moretti and Kays (1964) used an open-circuit wind tunnel, subsequently modified by Moffat (1967) and in use since 1967. This apparatus is shown in Fig. 5. It consists of a centrifugal blower followed by a heat exchanger for

controlling free-stream temperature, a set of calming screens, a two-dimensional contraction nozzle, and a test section. The upper surface of the test section can be adjusted to accomplish either acceleration or deceleration of the main stream. The lower surface consists of 24 individual calorimeter sections arranged to form a smooth plate 2.4 m long and 0.5 m wide which is uniformly porous ($\pm 6\%$ over the center 0.2 m span). Each individual porous element is instrumented to allow heat transfer rate to be determined by energy-balance means, based upon the measured electrical power and data concerning the heat losses by various modes. Installation details for the porous plates are shown in Fig. 8a. Transpiration flow, either blowing or suction, can be adjusted individually to each of the 24 test plates. The surface is made of sintered bronze powder and has been shown to be aerodynamically smooth (i.e., no roughness effects) at least up to air speeds of 38 m/s, above the usual testing range. The main stream flow is of moderate turbulence (0.25 to 0.5%), and the flow is sufficiently two-dimensional on the test plate that the momentum thickness is uniform within $\pm 3\%$ of the mean value over the center 0.2 m width of the test plate. All of the Stanford data for smooth plates (with and without transpiration) shown in this collection were taken with this same apparatus.

Figure 6 shows a schematic of the test tunnel used for studies of discrete-hole injection: normal, slant, and compound angle. Details of the installation of a single test plate typical of the Discrete-Hole Rig or the Curvature Rig are shown in Fig. 8b. The tunnel is closed-loop, driven by a centrifugal blower using a water-to-air heat exchanger to provide temperature stability. A three-dimensional nozzle, a calming section, and turbulence-reducing screens are fitted to the upstream end of the test section. The flow velocity is uniform within $\pm 3/8\%$ across the test duct. Boundary layer momentum thicknesses are uniform within $\pm 3\%$ of the mean, in the center 0.2 m span. The preplate and afterplate are parts of the main tunnel and serve to document both the approaching and departing flow field. The test section can be exchanged for either normal-, slant-, or compound-angle injection. When compound-angle injection is used, secondary flow is controlled by synchronized suction on one side-wall and blowing on the other. By this means, an infinite-width test section is simulated. The tunnel is operated at a slightly positive static pressure, to control leaks, and at ambient temperature, to control the thermal boundary layer growth. This tunnel was used for

all three studies of discrete-hole injection but has been disassembled and rebuilt as the test rig for curvature effects.

Figure 7 shows a plan view schematic of the Curvature Rig. It is a closed-loop tunnel whose convex test surface is a segment of a circular arc. The concave wall is set to a profile determined partly analytically and partly by trial and error, to achieve a condition of uniform static pressure along the convex working surface from the beginning of curvature to the end. Experiments have shown that the static pressure is uniform, along the test section, to within 3% of the free-stream dynamic head.

Curvature induces secondary flows, which make accurate experiments difficult. A development program was conducted to reduce the secondary flows, with good success. At present, the boundary layer flow on the curved test surface does not show convergence worse than $2-1/2^\circ$ at any location, in the worst flow case. This was accomplished by installing axial fences along the curved surface, 5 cm from the side walls. These fences protrude beyond the boundary layer, into the free stream, and isolate the side walls from the curved portion of the test rig.

This apparatus has been used to evaluate the effects of curvature on shear stress, turbulence structure, and heat transfer rate. All Stanford data pertaining to convex curvature have come from this piece of equipment.

The curved region is formed of twelve individual calorimeter sections, using the same design philosophy as used in the Discrete-Hole Rig, shown in Fig. 8b. In the Curvature Rig, however, the entire curved surface was machined to a constant radius as a last fabrication step.

A third tunnel, of the same basic geometry as the discrete-hole test tunnel, was built for studies of rough-wall behavior. The Roughness Rig was used for the works of Heazler (1974) and Pimenta et al. (1979). Its surface consists of a regular array of spherical elements, each 1.25 mm in diameter, brazed together to form 24 segments of porous, rough, test wall. The porosity and geometry are extremely uniform. The surface represents an idealized sand-grain roughness on a permeable surface. The test surface is 2.4 m long and 0.5 m wide. The crests of the spheres forming the surface are all aligned on the same plane. Transpiration flow is measured with hot-wire anemometer flow meters installed into the header tubes, one flow meter for each plate segment.

Throughout the Stanford program, velocities and turbulence quantities have been measured using boundary layer pressure probes or hot-wire anemometers. The objective has been to measure Stanton number within 0.0001 Stanton number units over the entire range of conditions. All of the test plates are calorimetric in nature except the pre- and afterplates in the Discrete-Hole Rig and the Curvature Rig; there, heat flux meters are used.

UNIFORM WALL TEMPERATURE

The baseline case for turbulent boundary layer heat transfer is a smooth plate of uniform temperature exposed to a steady two-dimensional flow of gas at a temperature nearly equal to that of the surface.

Many early researchers studied this case. The earliest work in the present program at Stanford was reported by Reynolds et al. (1958a). At that time, variable properties effects were principally dealt with using either a properties-ratio or a temperature ratio corrector based upon wall and free stream values; hence the plotted data include the correction factor $(T_w/T_\infty)^{0.4}$.

Figure 9 shows the principal output data from this study. The recommended correlation was

$$St = 0.0296 Re_x^{-0.2} Pr^{-0.4} \left(\frac{T_o}{T_\infty} \right)^{-0.4} \quad (12)$$

The data shown agree with this correlation for free stream velocities between 43 and 127 fps, and values of x-Reynolds number between 9×10^4 and 3.5×10^6 .

Over the years since 1958, this correlation has stood up well, and there seems little reason to doubt it.

VARIABLE WALL TEMPERATURE

If the temperature of a hot wall under a cold stream is increasing in the flow direction, the heat transfer coefficient will be higher than would exist on a wall of uniform temperature. Conversely, if the temperature of the wall is decreasing in the flow direction, the heat transfer coefficient will be lower.

Figure 10 illustrates the mechanism responsible for this result, when there exists a small step, ΔT_w , in wall temperature. The effect of the step in wall temperature is much greater on $\partial T/\partial y|_0$ than on $(T_w - T_\infty)$; hence the value of h increases. A gradual increase can be modeled as a sequence of steps and results in an increase in h , while a gradual decrease in wall temperature represents a sequence of steps down in temperature, and results in low values of h .

For constant properties flow, with no buoyancy effects or chemical reaction, the energy differential equation is linear in temperature. Hence, arbitrary temperature boundary conditions can be treated by the method of superposition, once the response of the boundary layer to a step in wall temperature is known.

Reynolds et al. (1958b) presented a kernel function for superposition treatment of variable wall temperature effects as:

$$\frac{St}{St_T} \Big|_{Re_x} = \left[1 - \left(\frac{\xi}{\bar{x}} \right)^{9/10} \right]^{-1/9} \quad (13)$$

or

$$St = 0.0296 Re_x^{-0.2} Pr^{-0.4} \left(\frac{T_w}{T_\infty} \right)^{-0.4} \left[1 - \frac{\xi}{\bar{x}} \right]^{-1/9} \quad (14)$$

The data which this analysis is intended to model are shown in Fig. 11. The agreement is good except very near the step, say, for example, for a few (five or six) boundary layer thicknesses. The data show that this kernel function can be used for both thick and thin boundary layers, since boundary layer thickness is properly accounted for by use of $St_T|_{Re_x}$, the Stanton number expected for a uniform wall temperature at the same x -Reynolds number.

Figure 12, taken from Whitten (1967), shows a comparison of measured and predicted Stanton numbers for a rather complex situation. The free stream velocity was held uniform, but the plate was subjected both to variable transpiration and to variable wall temperature. The transpiration varied linearly with X according to

$$\frac{v_0(X)}{U_\infty} \triangleq F(X) = 0.00005X \quad (15)$$

Simultaneously, the temperature of the wall followed the profile at the top of the figure: uniformly 50° F hotter than the gas from $Re_x = 0$ to $Re_x = 5.5 \times 10^5$, an abrupt step down to 23° F above gas temperature from $Re_x = 5.5 \times 10^5$ to $Re_x = 1 \times 10^6$, followed by a linear rise to about 65° F above gas temperature. Measured values of Stanton number are shown by the squared symbols, while the line through the squares represents the result of an integral analysis based upon the superposition kernel, and accounting for both the effects of transpiration and variable wall temperature. The solid curve labeled $F = 0$ represents the Stanton number expectation for a uniform temperature surface with no transpiration.

ACCELERATION EFFECTS

The Stanford work on acceleration effects began with Moretti and Kays (1964), who reported substantial decreases in local Stanton number as a consequence of acceleration of the main stream. Acceleration was measured in terms of

$$k \triangleq \frac{v}{U_\infty^2} \frac{dU_\infty}{dx}, \quad (16)$$

as suggested by examination of the momentum integral equation. The accelerations examined consisted of some abrupt and some sustained accelerations. In every case, the Stanton number decreased rapidly under acceleration. The phenomenon was described as "re-laminarization", in the literature of that period, based upon the similarity to laminar behavior.

Subsequent work showed a complex interaction between acceleration, transpiration, and the initial conditions. Successful predictions were achieved

with a finite-difference predictor program, however, by the expedient of allowing the van Driest damping parameter, A^+ , to be a function of both p^+ and v_0^+ . The form of this relationship is presented in the section on modeling.

The experiments which followed Moretti and Kays concentrated on flows with constant K , as they represent potentially asymptotic (equilibrium) boundary layers. Hydrodynamic investigations by Julien et al. (1969) showed an asymptotic momentum thickness for each value of K . Following this lead, flows were established for several different values of K , each with its appropriate initial momentum thickness. By this means, a long run at equilibrium was attained, and the self-preserving structure of the boundary layer identified. Velocity and temperature profiles, and turbulence data, were taken and used to develop the model functions for the predictor program.

Figure 13 shows the effects of moderate and strong acceleration on the Stanton number for a smooth plate with no transpiration. Significant depression of the Stanton number was achieved, and the response is orderly with increasing K value. The slope of the Stanton number curve approaches laminar behavior (i.e., decreasing with $Re_x^{0.5}$) for K values of 2.5×10^{-6} . This corresponds to a slope of -1 for enthalpy thickness Reynolds number coordinates, as in Fig. 13. This has been taken as the "relaminarization" value of K . The evidence is that turbulence still exists in the boundary layer, however, in spite of the rapid drop in Stanton number.

It has been shown, by computer experiments, that this drop in Stanton number can be predicted by letting A^+ , the van Driest damping constant, increase with acceleration, in effect thickening the laminar sublayer.

Figure 14 introduces transpiration to a boundary layer with moderate acceleration, $K = 0.77 \times 10^{-6}$. With no blowing, there is essentially no effect on Stanton number, but with blowing at $F = +0.006$, Stanton number is increased (compared at constant enthalpy thickness Reynolds number). With suction at $F = -0.002$, Stanton number is decreased. These are opposite to the separate effects: with no acceleration, blowing decreases Stanton number, while suction increases it.

It appears that the two mechanisms, acceleration and blowing, act in opposition to one another. One explanation might be that blowing tends to

decrease the thickness of the sublayer, while acceleration tends to increase it.

Figure 15 shows the effect of initial conditions on the response of a boundary layer to strong acceleration. The solid line represents laminar behavior.

DECELERATION

In contrast to the dramatic effects of acceleration, deceleration causes only small changes in the boundary layer behavior. Extensive tests have been conducted with deceleration coupled with blowing and suction, by Blackwell (1972) and Orlando (1974). Figure 16 shows data for a moderate deceleration ($m = -0.15$) with blowing up to $F = +0.004$ and suction to -0.004 . The solid lines are the correlations for constant-velocity flow, for the same value of blowing. The data points for decelerating flows lie exactly along the constant velocity correlation lines.

The conclusion one must draw from this is that there is little or no effect of a positive pressure gradient upon the thickness of the sublayer of the boundary layer. In terms of the damping constant, this means that A^+ is relatively insensitive to positive values of the pressure gradient.

From the standpoint of integral solutions, deceleration has no significant effect on the relationship between Stanton number and enthalpy thickness Reynolds number.

FREE STREAM TURBULENCE

A representative collection of experiments on the effects of free stream turbulence is given by the works of Kestin (1966), Kearney et al. (1970), Slanciauskas and Pedesius (1977), Brown and Burton (1978), Bradshaw and Simonich (1978), and Blair (1983).

Kestin reported no effect of turbulence level on a constant-velocity turbulent boundary layer. Kearney et al. reported no effect on the constant-velocity boundary layer and also no effect when a strong acceleration was

applied to the flow ($K = 2.5 \times 10^{-6}$) for a turbulence level of 4%. Slančiauskas and Pedesius found effects of 10% to 15% with turbulence intensities up to 8%, but obtained a 20% increase when the turbulence intensity rose to 14%. Part of this increase was attributed to changes in the main stream flow as a consequence of the boundary layer growth. Brown and Burton confirmed Kestin's results; but then, in 1978, Simonich and Bradshaw reported an increase in Stanton number in response to free stream turbulence. This was followed in 1983 by other work which also showed an increase.

Kestin concluded that the principal effect of inducing free stream turbulence of 3.8% was to move the transition location upstream. He found no effect on the fully developed turbulent layer. This study was confirmed by Kearney et al. (1970), at Stanford. Their data are shown in Fig. 17. Kearney's test section consisted of a duct with a flat-plate floor and a top wall which could be adjusted to produce either a uniform velocity flow or an acceleration at constant K . A uniform velocity section followed the accelerating section. Data were taken in all three sections of the plate, for a low-velocity (6-18 M/s) flow in the tunnel.

Kearney's data for low (0.7%) and moderate (3.9%) turbulence show no effect on Stanton number. The two data sets are well aligned with each other and agree with the constant-velocity correlation in the approach section. The STAN5 program was fitted with a turbulence kinetic energy closure and produced results which matched the data: no effect on Stanton number for 4% turbulence. Computer runs for 10% free stream turbulence, however, indicated a small increase in Stanton number, about 5%.

Slančiauskas and Pedesius tested over a wider range of turbulence levels (1.1% to 13.5%) but tested only the constant-velocity case. Their data are shown in Fig. 18. The effect of turbulence level is clearly discernible and orderly, and suggests an effect approaching 20% on Stanton number. These were the first data to suggest a significant effect due to turbulence.

Simonich and Bradshaw report larger effects, as shown in Fig. 19. Their data for heat transfer coefficient represent average values over a flat plate of relatively large size, and it is possible that increasing the turbulence caused a change in the location of the transition zone on the plate. One would expect high turbulence levels to cause the transition location to move upstream, raising the average heat coefficient on the plate by exposing more

Transition on a rough plate, with blowing, is illustrated in Fig. 23. Here, at a constant velocity of 9.8 M/s, Stanton number data were taken at successively higher values of the blowing fraction, $F = \dot{m}''/G$. The value of the momentum thickness at transition is noted at the bottom of each transition valley. The same value, about 400, obtains for rough surfaces with blowing, as is used conventionally for smooth, impermeable surfaces. Thus, neither roughness nor transpiration affected the location of the transition, in these coordinates.

Acceleration of the flow over a rough surface causes a different effect than does acceleration over a smooth plate. Figure 24 shows data from Coleman et al. (1976) for acceleration on a rough plate at constant K_R , the acceleration parameter for rough surfaces. Since the fully rough boundary layer is independent of velocity, it requires a different parameter to represent an equilibrium state.

Coleman showed that the general form of this acceleration parameter should be

$$K_r = \frac{L}{U_\infty} \frac{dU_\infty}{dx} \quad (18)$$

where L is a length scale of the surface roughness. Specifically, for the deterministic surface he used:

$$K_r = \frac{r}{U_\infty} \frac{dU_\infty}{dx} \quad (19)$$

where r , the length scale, was the radius of the spheres forming the surface.

When a flow accelerates along the rough surface at constant K_r , Stanton number increases, though not much. The increase is somewhat augmented by blowing. Overall, the effects of acceleration and blowing on a rough wall are much less important than those effects on a smooth wall. This supports the notion that both acceleration and transpiration act on the sublayer. Fully rough turbulent boundary layers display fully turbulent characteristics as near to the surface as measurements can be made, and act as though they have no sublayer.

SURFACE ROUGHNESS

Surface roughness increases both the friction factor and the Stanton number on a surface with a turbulent boundary layer. Roughness is generally appraised in terms of the roughness Reynolds number.

$$Re_k \triangleq \frac{U_\tau k_s}{\nu} \quad (17)$$

where U_τ = friction velocity, $\sqrt{\frac{g_c \tau_o}{\rho}}$,
 k_s = equivalent sand-grain roughness of the surface,
 ν = kinematic viscosity.

When the roughness Reynolds number is less than 5, the flow is regarded as smooth, when over 70, fully rough, and in between, transitionally rough.

Early work reported by Nikuradse (1950) showed the friction factor to be independent of free stream velocity — a function of distance alone. It was not surprising, therefore, that Moffat, Healzer, and Kays (1978) reported the Stanton number to be independent of velocity. Figure 21 shows Stanton number data plotted as a function of the enthalpy thickness of the boundary layer, made dimensionless by using the diameter of the particles forming their rough surface. Healzer's surface was made up of spherical copper elements, brazed together in a regular array to form a porous surface with a deterministic roughness: an idealized sand-grain surface. Friction factor tests showed this surface to behave as a classical sand-grain surface, based upon Schlichting's library of shapes tested (Schlichting, 1968).

If the Stanton number is a function of distance along the plate, it can also be described as a function of enthalpy thickness alone — independent of velocity. The fully rough state is expected to have this property, and Fig. 21 illustrates that the data behave as expected.

Less certain, however, is the effect of blowing. Blowing reduces the surface shear stress, hence reduces the roughness Reynolds number, and might be expected to produce a return to "smooth wall" behavior. Figure 22 shows Stanton number data for a range of blowing values up to $F = 0.008$. The Stanton number remains independent of velocity except, perhaps, for the runs at 32 fps (9.8 m/s), which deviate at high blowing. Thus a rough surface tends to remain rough with blowing.

Transition on a rough plate, with blowing, is illustrated in Fig. 23. Here, at a constant velocity of 9.8 M/s, Stanton number data were taken at successively higher values of the blowing fraction, $F = \dot{m}''/G$. The value of the momentum thickness at transition is noted at the bottom of each transition valley. The same value, about 400, obtains for rough surfaces with blowing, as is used conventionally for smooth, impermeable surfaces. Thus, neither roughness nor transpiration affected the location of the transition, in these coordinates.

Acceleration of the flow over a rough surface causes a different effect than does acceleration over a smooth plate. Figure 24 shows data from Coleman et al. (1976) for acceleration on a rough plate at constant K_R , the acceleration parameter for rough surfaces. Since the fully rough boundary layer is independent of velocity, it requires a different parameter to represent an equilibrium state.

Coleman. showed that the general form of this acceleration parameter should be

$$K_r = \frac{L}{U_\infty} \frac{dU_\infty}{dx} \quad (18)$$

where L is a length scale of the surface roughness. Specifically, for the deterministic surface he used:

$$K_r = \frac{r}{U_\infty} \frac{dU_\infty}{dx} \quad (19)$$

where r , the length scale, was the radius of the spheres forming the surface.

When a flow accelerates along the rough surface at constant K_r , Stanton number increases, though not much. The increase is somewhat augmented by blowing. Overall, the effects of acceleration and blowing on a rough wall are much less important than those effects on a smooth wall. This supports the notion that both acceleration and transpiration act on the sublayer. Fully rough turbulent boundary layers display fully turbulent characteristics as near to the surface as measurements can be made, and act as though they have no sublayer.

Pimenta (1979) made an extensive study of the structure of turbulence in a fully rough boundary layer flow, documenting the mixing length and turbulent Prandtl number distribution.

TRANSPIRATION

Experiments describing the effects of transpiration on surface heat transfer were first reported by Mickley, Ross, Squyers, and Stewart (1954). These results were superseded by a second series of measurements in 1957 (Mickley and Davis, 1957), and followed by Kendall (1959), Favre et al. (1966), and Torii, Nishiwaki, and Hirotsu (1966), who extended the range of data and confirmed the trends reported by Mickley and Davis.

The Stanford program began in 1966 with a study of blowing and suction through a smooth, uniformly porous plate, reported by Moffat (1967). The data are shown in Fig. 25 in terms of Stanton number versus x -Reynolds number for a range of values of \dot{m}''/G from -0.0076 to $+0.0096$.

At \dot{m}''/G of -0.0076 , the boundary layer is in an asymptotic state due to the strong suction. The boundary layer thickness does not increase in the streamwise direction, and the Stanton number is both constant and numerically equal to $(-\dot{m}''/G)$.

The data for $\dot{m}''/G = -0.0046$ show the approach to asymptotic behavior. For x -Reynolds numbers less than 10^6 , the boundary layer is growing and the Stanton number is decreasing until a condition is reached where Stanton number and \dot{m}''/G are equal. From that point on, an asymptotic state persists.

At high blowing, $\dot{m}''/G = +0.00955$, the Stanton number decreases rapidly towards zero and the boundary layer can be said to be "blown off" the surface. Diffusive transport to the wall is essentially zero.

The effects of transpiration can be seen in a different light in Fig. 26, which presents Stanton number as a function of \dot{m}''/G for several different Reynolds numbers. Figure 26 shows the limits of boundary layer behavior when transpiration is present. Note the approach to the suction asymptote, at large suction rates, and the gradual approach to zero Stanton number at high blowing.

In many cases, x -Reynolds number is not an appropriate descriptor of boundary layer condition. The preceding data for Stanton number are presented in Fig. 27 in purely local coordinates: Stanton number versus enthalpy thickness. For a constant properties flow,

$$\Delta_2 = \int_0^{\infty} \frac{\rho u}{\rho_{\infty} u_{\infty}} \left(\frac{t - t_{\infty}}{t_0 - t_{\infty}} \right) dy \quad (20)$$

The enthalpy thickness, Δ_2 , has been found useful in correlating heat transfer data under conditions of accelerating and decelerating flow, or whenever the boundary conditions change in the x -direction.

The choice of constant \dot{m}''/G along the surface was arbitrary. One could equally well choose to test under conditions of a constant blowing parameter, B_h , defined on the basis of the energy integral equation, shown below for a two-dimensional, constant-properties, constant-velocity flow on a flat plate of uniform temperature.

$$St + \frac{\dot{m}''}{G} = \frac{d\Delta_2}{dx} \quad (21)$$

becomes

$$St(1 + B_h) = \frac{d\Delta_2}{dx} \quad (22)$$

where

$$B_h = \frac{\Delta}{GSt} \frac{\dot{m}''}{GSt}$$

Testing at constant B_h fixes the ratio between the rate at which energy is diffused from the wall as heat transfer to the rate at which energy is carried from the wall by the transpiration gas. When the ratio of these two is fixed, the boundary layer behavior is different than when only one of the conditions is fixed.

Whitten (1967) conducted a series of tests with constant B_h along the test plate and showed that the behavior of the boundary layer was essentially the same, at a given point, regardless of whether that point had been reached along a path of constant B_h or constant F . This demonstration of purely local behavior supports the integral approach to boundary layer approximation: the upstream history evidently has only a secondary effect on behavior at a point.

It is desirable to have an estimator for the local effects of blowing. Couette flow analysis predicts:

$$\left. \frac{St}{St_o} \right|_{Re_x} = \frac{\ln(1+B)}{B} \quad (23)$$

where $St \stackrel{\Delta}{=} Stanton$ number with blowing.

In view of the number of assumptions required to arrive at Eqn. (23) from a Couette flow analysis, it is a surprisingly accurate predictor. Figure 28 compares measured values of St/St_o , at constant x -Reynolds number, to the local value of $\ln(1+B)/B$. For all positive values of B , the agreement is excellent.

Whitten (1967) used Eqn. (23) with the two-dimensional integral equation to derive the equivalent form expressed in terms of the enthalpy thickness Reynolds number, for smooth-surface flows:

$$\left. \frac{St}{St_o} \right|_{Re_{\Delta_2}} = \left[\frac{\ln(1+B)}{B} \right]^{1.25} (1+B)^{0.25} \quad (24)$$

Moffat et al. (1978) showed the local effects of blowing on a fully rough boundary layer to be given by:

$$\left. \frac{St}{St_o} \right|_{\Delta_2} = \left[\frac{\ln(1+B)}{B} \right]^{1.25} (1+B)^{0.25} \quad (25)$$

DISCRETE HOLE INJECTION

Discrete-hole injection and slot injection are alternatives to transpiration. They are attractive from the standpoints of manufacturing and strength, and offer flexibility in design which transpiration does not.

Injection through large holes or slots opens up the possibility that the injected fluid will be at a temperature different from the surface or the free stream. The heat transfer problem thus becomes a three-temperature-potential problem, with one degree of freedom not usually found in heat transfer problems. This has been addressed by some workers in the field by assigning a "surface effectiveness" to the injection process and calculating the surface temperature as a function of injection rate and injection temperature. This

reduces the heat transfer problem to a two-potential problem. Typically, following the effectiveness approach, the heat transfer coefficient used in the final calculation far downstream of injection is taken from standard correlations with no injection, based on either x -Reynolds number or enthalpy thickness Reynolds number. This method is surely adequate far downstream from the injection site, where the boundary layer has returned to normal hydrodynamics. One must have some reservations, however, about whether or not this approach is valid within a region of full-coverage film cooling, or even in the near-downstream region, where the velocity and temperature distributions are far from normal.

As a consequence of these reservations, the Stanford program has adopted a different approach. The problem of calculating surface heat transfer rate is postulated as a two-temperature-potential problem, with the heat transfer coefficient containing both the effects of the fluid mechanics and the third temperature potential. Actual gas temperature and actual wall temperature are used for the driving potential for heat flow:

$$\dot{q}'' = h(T_{\infty} - T_{wall}) \quad (26)$$

where $h = h$ (fluid mechanics, temperature level of injection).

The analytical basis for this approach was described by Choe et al. (1975). Briefly, the argument is as follows. Consider a surface with an array of holes or slots injecting coolant at some fixed rate into a boundary layer. Let all of the hydrodynamic conditions be independent of the temperature of the free stream, the wall surface, or the injection temperature. Now, consider the energy equation applicable to this domain. For constant fluid properties, the energy equation will be linear and superposition can be used. Consider two basic data sets: one for the injected fluid at wall temperature ($\theta = 1.0$) and one for the injected fluid at free-stream temperature ($\theta = 0.0$). For each case, at every point on the surface, there will exist a certain heat transfer rate, and, for each case, a local Stanton number can be defined. The Stanton numbers for $\theta = 0$ and $\theta = 1.0$ can be combined to describe the Stanton number for any arbitrary value of θ , by the following relationship:

$$St_{\theta} = St_{(0)} + \theta \{ St_{(0)} - St_{(1)} \} \quad (27)$$

where

$$\theta = \frac{t_{inj} - t_{\infty}}{t_0 - t_{\infty}} \quad (28)$$

and

$$St_{(0)} \stackrel{\Delta}{=} \text{value of Stanton number when } \theta = 0 \quad .$$

$$St_{(1)} = \text{value of Stanton number when } \theta = 1 \quad .$$

In fact, the experimental values of $\theta_{(0)}$ exceed those of $St_{(1)}$ so that the equation is usually used as:

$$St_{\theta} = St_{(0)} - \theta \{St_{(0)} - St_{(1)}\} \quad (29)$$

This process is illustrated in Fig. 29, which also shows the relationship between the concept of the superposition approach and the concept of the adiabatic wall effectiveness. The injection temperature which achieves an adiabatic wall condition ($St = 0$) defines the effectiveness.

Regardless of which approach is used, two pieces of information are needed for each calculation: either h and n or $h_{(1)}$ and $h_{(0)}$. It can be shown that $h_{(0)}$ from the superposition approach is the appropriate value to use for h in the effectiveness approach, when calculating within the near field of the jets.

Some questions arise when considering the use of low-temperature, low-speed data in predicting performance in high-temperature, high-speed flows. First, what should be held constant in extrapolating to engine conditions:

$$\frac{\rho_0 v_0}{\rho_{\infty} U_{\infty}}, \quad \frac{\rho_0 v_0^2}{\rho_{\infty} U_{\infty}^2}, \quad \frac{v_0}{U_{\infty}}, \quad \text{or} \quad \frac{Re_{jet}}{Re_{flow}} \quad ?$$

At present there is no definitive answer. Second, when considering a "set" of data (i.e., one value of h and one value of n or one value of $h_{(0)}$ and one of $h_{(1)}$), how does one "hold constant" the hydrodynamics? Both methods require that the two members of the set be appropriate for the same "predicted case", but the thermal conditions for the two members are necessarily different and will affect the hydrodynamics; thus they cannot be the same. Careful experiments are required at scale and real conditions.

The superposition approach defines an h value which is a function of the injection rate and the injectant temperature, and two data sets are needed, $(St_{(1)})$ and $(St_{(0)})$, to account for both thermal and fluid mechanic effects. All of the Stanford data will be presented in this format.

Figures 30-32 show Stanton number data for three different injection geometries: normal, 30° slant, and 30° slant with 45° yaw. Data are presented for $\theta = 0$ and $\theta = 1.0$ over a range of injection parameters including a baseline with no injection. The injection parameter used is:

$$M \triangleq \frac{\rho_o U_o}{\rho_\infty U_\infty} \quad (30)$$

The pitch-to-diameter ratio is 5 for all three figures, and the free-stream velocity about 55 fps (16.7 m/s). There is one difference in the test conditions which is relevant: the compound-angle injection data were taken with a heated initial plate (i.e., thick thermal boundary layer), whereas the normal and slant-injection data were taken with no upstream heating (i.e., a thin thermal boundary layer). A thick thermal boundary layer responds differently to injection than does a thin boundary layer, and the compound injection data for $\theta = 1.0$ would be a few percent higher (i.e., a few percent less favorable) had those tests been done with a thin thermal boundary layer.

The first data point (lowest x -Reynolds number) in each set has no blowing, and the open-circle data symbols represent the no-blowing behavior of the test plate. Whenever the $\theta = 1$ data lie above the unblown data, the surface heat transfer has been increased even though wall-temperature fluid was injected. This increase represents one of the two effects of injection: increasing the level of turbulent mixing within the boundary layer. If the injection rate is too high, the early portions of the protected surface will actually encounter an increase in heat transfer, even though the injected fluid is at wall temperature, as a consequence of this increased mixing.

For each geometry there exists an optimum value of M for $\theta = 1.0$, in the vicinity of $M = 0.4$ to $M = 0.6$, depending upon the geometry. If the injection rate goes above the optimum, the Stanton number goes up.

Each data set presented here consists of twelve data points within the full-coverage region, followed by six or more data points in the region down-

stream of the full-coverage region--the recovery region. The recovery region may be as important as the full-coverage region.

It can be seen from Figs. 30-32 that compound-angle injection reduces the Stanton number to lower values than either slant or normal injection, but that the recovery to flat-plate behavior is more rapid.

Figure 33 presents a direct comparison of slant-angle data (Crawford et al., 1976) with compound angle (Kim, 1979). The thermal and hydrodynamic entrance conditions of the test were substantially identical. The advantage of compound-angle injection is found in the downstream portion of the full-coverage region and the early portion of the recovery region.

Figure 34 shows typical data for compound-angle injection with $P/D = 10.0$. For a given amount of injected fluid, $P/D = 10$ offers much less thermal protection. It appears that $P/D = 10$ increases the turbulent mixing without providing a compensatory thermal benefit.

There are distinct problems involved in trying to model the heat transfer distribution on a surface with a region of full-coverage film cooling followed by a recovery region. The approach followed at Stanford has been to define and measure the spanwise-averaged properties of the boundary layer and treat the problem as pseudo-two-dimensional. This introduces some experimental complexity, but has proven adequate for predicting most of the effects of injection. The details of the model will be discussed in a later section, along with an example of the agreement between predicted and measured Stanton numbers.

SURFACE CURVATURE

Even though there were some warnings in the literature in the early 1930s, it was not until the work of Thomann (1958) that the boundary layer heat-transfer community sat up and began to take notice of surface curvature as a significant variable. His results (Fig. 35) showed a 20% increase in heat transfer for concave curvature and a comparable decrease for convex curvature for supersonic flow. The increase for concave flows was attributed, in part, to streamwise vortices similar to the Taylor-Görtler vortices seen in

concave laminar boundary layers. Mayle, Blair, and Kopper (1979) showed similar findings, in subsonic tests.

Simon et al. (1980) conducted an exhaustive study of strong curvature ($\delta_{0.99}/r = 0.10$) in combination with other effects: changes in $\delta_{0.99}/r$, changes in U_∞ , free-stream acceleration changes in boundary layer maturity. They found that $\delta_{0.99}/r$ is not a strong factor in determining heat-transfer behavior, for values between 0.02 and 0.10. This suggests that, once some lower critical value is passed (perhaps $\delta_{0.99}/r = 0.02$), the boundary layer no longer responds to further changes. The heat-transfer Stanton number was only a weak function of free-stream velocity. A significant finding was that, when Stanton number was plotted against enthalpy-thickness Reynolds number (Re_{Δ_2}), the data displayed a slope of -1 throughout the convexly curved region. This has been taken to be the distinguishing signature of strong curvature. Results from this study are shown in Figs. 36 and 37, which show the same data in x -Reynolds number and enthalpy-thickness Reynolds number. The values of enthalpy-thickness Reynolds number were calculated from the Stanton number data using the two-dimensional energy integral equation.

The strongest effect found was due to free-stream acceleration. Figures 38 and 39 show the combined effects of moderate acceleration with strong curvature. These runs were conducted at constant K throughout the curved region. The hydrodynamic boundary layers were at equilibrium thickness for the proposed value of K at the onset of curvature. It is noteworthy that large effects were found even though the values of K used were not large enough to have significantly affected a flat (i.e., uncurved) boundary layer. Of particular interest is the effect shown in Fig. 39, where the slope is -2 within the curve, for $K = 1.25 \times 10^{-6}$. Acceleration at $K = 3 \times 10^{-6}$ is known to result in a slope of -1 in these coordinates, on a flat surface. Emergence of the -2 slope suggests that curvature and acceleration act on different regions of the boundary layer, since their effects appear to be additive.

Convex curvature was shown to retard, but not prevent, transition from a laminar to a turbulent boundary layer.

Figure 40 shows shear stress profiles from Gillis et al. (1980). Wall shear drops immediately inside the curved region, and remains low throughout

the curve. The subsequent recovery region shows low shear stress (and heat transfer) extending as far downstream as 20-50 boundary-layer thicknesses.

The recovery region is of importance in gas turbine heat transfer, because of the slow recovery. Slow recovery here means good thermal protection; Stanton number is low and remains low in the recovery region for a long run.

FREE AND MIXED FREE AND FORCED CONVECTION

Experiments on high Grashof number, high temperature-difference, free convection were reported by Siebers, Schwind, and Moffat (1983). These experiments involved a large (3 m x 3 m), vertical test plate operated at temperatures up to 600°C in free convective and mixed convection (i.e., with a horizontal flow) up to 6 m/s.

Baseline tests in pure free and pure forced convection agreed with accepted correlations within 2% over the range of existing correlations, and mean velocity and mean temperature profiles also agreed with expectations.

Figure 41 shows free convection Nusselt numbers for Grashof number up to 2×10^{12} , the highest value in the literature. Fluid properties were evaluated at "free stream" temperature, not at "film temperature" or any other intermediate value. This collects the data very well, and only a very small correction is needed, even for the very high-temperature data. In contrast, had the data been reduced using fluid properties evaluated at the wall temperature, a large correction would have been needed.

Figures 42, 43, and 44 show different aspects of the mixed convection data. Figure 42 shows the average Nusselt number as a function of Reynolds number and Grashof number. The average Nusselt number was calculated from 105 individual measurements, spread uniformly over the surface. However, transitional and turbulent regions are all included in the average. Lines of constant Gr/Re^2 are shown demarcating the domains of pure free and pure forced convection. If the ratio Gr/Re^2 is equal to or less than 0.7, the situation can be treated as pure forced convection, while for $Gr/Re^2 > 10$, pure free convection correlations apply. Only between 0.7 and 10.0 is a "mixed-convection" correlation necessary. In this region, one can calculate the

average heat transfer by a combination of the appropriate expression for pure free and pure forced convection given below:

$$h_{\text{mixed}} = \{h_{\text{free}}^3 + h_{\text{forced}}^3\}^{1/3} \quad (31)$$

The distribution of local h is illustrated in Figs. 43 and 44. Each figure shows the distribution of h for five different combinations of wall temperature and free stream velocity. Each of the two asymptotic states has its characteristic distribution of h . Pure free convection shows uniform h everywhere on the plate, while pure forced convection shows three regions: laminar, transitional, and turbulent. There is, in both composites, a smooth transition between distributions.

UNSTEADY EFFECTS

One characteristic of the flow field on turbine vanes and blades is a periodic, unsteady component related to blade passing frequency. It has often been suggested that this unsteady behavior will affect heat transfer.

The effect of pulsating flow on heat transfer in tubes was reviewed by Yen (1977), who found, of 52 references, approximately 1/3 claiming an increase in heat transfer coefficient, 1/3 claiming a decrease, and 1/3 reporting no effect. Yen's experiment consisted of pulsing a turbulent tube flow at a frequency close to the bursting frequency predicted for the time-averaged Reynolds number. A very small decrease in h was found--less than 11% in any case.

Feller (1964) reported that 100 Hz pulsations in the flow velocity increased the heat transfer coefficient on a flat plate, but only by causing the laminar/turbulent transition zone to move upstream, exposing more of the plate to turbulent flow. This effect is the same as Kestin reported for the effect of free stream turbulence.

There is, at present, no clear evidence that periodic variation in the free stream velocity alters the heat transfer except by relocating the transition line.

SECONDARY FLOWS

End-wall surfaces in vane and blade rows are subject to pressure gradients normal to the main stream flow. This results in the bounding streamline for the sublayer having a different direction than the free stream. There is, at present, no systematic study of this problem.

The difficulties are well illustrated by the results reported by Georgieu et al. (1979). They show contours of constant "h" on the end wall of a turbine cascade and discuss three correlation schemes: tracking a potential streamline, defining a bulk average, and chordwise application of the energy integral equation. None was successful within 50% in correlating the heat transfer.

Large lateral variations in heat transfer coefficient were reported, about 1.6 to 1 across the passage, with high values near the suction side and low values near the pressure side. The distribution could be altered by free stream turbulence and by boundary layer thickness.

MODELING

The final objective of heat transfer experiments is to develop the ability to predict. Accordingly, it is as important to extract the modeling information as it is to measure heat transfer.

The principal tool for prediction, in the Stanford Heat and Mass Transfer Program, is the STAN5 program (Crawford & Kays, 1976), which uses the Prandtl mixing length with a modified van Driest damping parameter, A^+ . This augmented mixing length concept allows calculation of the distribution of the mean velocity, including effects of pressure gradient and blowing. Heat transfer calculations can be made only after the proper mean velocity profiles have been deduced. The calculation of heat transfer rate also requires data concerning the turbulent Prandtl number. Thus the principal modeling efforts are aimed at A^+ and Pr_T in the Stanford data.

Present research seems heading towards use of closures based on turbulence intensity, and it seems only prudent to store data concerning the

turbulence intensity, as support for future models. Most of the recent data sets include turbulence measurements.

The mixing length can be thought of as having three different zones: the sublayer region, the y -proportional region, and the outer region.

Predicting boundary layer behavior with a finite-difference program involves one in many small but important details. The only way to transmit all of the relevant detail is to transmit a copy of the actual computer code. The comments which follow treat only the main physical elements: the modeling of A^+ and Pr_T . These represent the proper physical inputs for a general mixing length approach for slowly varying boundary condition. The details of how to ensure stability, convergence, and proper response to abrupt changes in boundary condition can be found in the STAN5 program, described by Crawford and Kays (1976).

The undamped mixing length region, where $\lambda = 0.41 y$, seems to be a generally valid concept. Data from accelerating, decelerating, smooth, rough, and transpired boundary layer all show the same feature: a region wherein $\lambda = 0.41 y$. Figure 45 shows mixing length data extracted from decelerating flows with blowing and suction. Similar results were found in accelerating rough-wall flows with and without blowing.

The damped region, near the wall, proposed by van Driest, can be greatly extended in utility if the parameter A^+ is allowed to be a function of v_o^+ and p^+ .

$$A^+ = \frac{25}{a \left[v_o^+ + b \left(p^+ / 1 + c v_o^+ \right) \right] + 1} \quad (32)$$

where $a = 7.1$ if $v_o^+ \geq 0.0$, else $a = 9.0$,
 $b = 4.25$ if $p^+ \leq 0.0$, else $b = 2.9$,
 $c = 10.0$ if $p^+ \geq 0.0$, else $c = 0.0$.

Equation (32) is suitable for all smooth-wall work and has been shown (Kays and Moffat, 1975) to be successful in predicting combinations of acceleration and blowing, as well as decelerations and flat-plate flows. Figure 46 shows A^+ versus p^+ and v_o^+ from Eqn. (32).

The outer region is characterized by:

$$\ell = 0.084 \delta_{0.99} \quad (33)$$

Turbulent Prandtl number data for a smooth, flat-plate flow with blowing and suction are shown in Fig. 47. The value tends towards $1/Pr$ at the wall and 0.5 in the outer region. The mid-range value is approximately unity. Either of the following equations seems adequate (Kays and Moffat, 1975).

$$Pr_t = 1.43 - 0.17 (y^+)^{1/4} \quad (34)$$

(but Pr_t should not be less than 0.86)

or

$$Pr_t = 0.90 + 0.35 [1 + \cos(\pi y^+/37)] \quad \text{for } y^+ \leq 37 \quad (35)$$

$$Pr_t = 0.90 \quad , \quad 37 < y^+ < \frac{\lambda \delta_{0.99}}{\kappa}$$

$$Pr_t = 0.60 \quad , \quad y^+ > \frac{\lambda \delta_{0.99}}{\kappa}$$

where $\lambda = 0.084$ and $\kappa = 0.41$.

Rough walls have been studied by Pimenta (1979) and Ligrani (1979). The mixing length follows the original Prandtl form in the undamped region, but an interesting region lies near the wall. Here, instead of approaching zero, as conventional mixing-length theory dictates, rough-wall boundary layers tend toward a non-zero value at the wall. Ligrani (1979) gives, for fully rough flows:

$$\ell = 0.41 \left[y + .0307 k_s \left(1 - \frac{Re'_k}{Re_k} \right) \right] \quad (36)$$

where k_s = equivalent sand-grain roughness,

Re_k = roughness Reynolds number, $u_\tau k_s / \nu$,

Re'_k = value of roughness Reynolds number at which the fully rough state is attained for the surface in question.

Since $Re_k = Re'_k$ for fully rough flow, the mixing length remains non-zero at the wall.

When a rough wall with transpiration is encountered, Ligriani recommends:

$$\ell = 0.41 \left[y + 0.0307 k_s \left(1 + 16.0 \psi \frac{v_o}{u_\tau} - \frac{u'_\tau}{u_\tau} \right) \right] \quad (37)$$

where: k_s = equivalent sand-grain roughness,

$\psi = 1.0$ if $Re_k > 55$,

$\psi = Re_k/55.0$ if $Re_k \leq 55.0$,

v_o = blowing velocity,

u_τ = shear velocity, $\sqrt{\tau_o/\rho}$,

u'_τ = shear velocity at the onset of fully rough behavior.

Equation (37) simulates the experimentally obtained result, that blowing seems to enhance roughness--not suppress it.

For transitionally rough flows (flows where Re_k is less than 55), some damping of the mixing length is observed. The damping parameter, A_R^+ , is given by Ligriani as:

$$A_R^+ = A^+ \{1 - g(Re_k)\} \quad (38)$$

where the g function depends upon the angularity and regularity of the roughness elements in a complex manner.

One of the most identifiable characteristics of roughness is the change it causes in the mean velocity distribution expressed in "inner coordinates", i.e., u^+ versus y^+ . The lag region of a rough-wall profile is depressed below the smooth-wall line by an amount which can be correlated with the roughness Reynolds number. A frequently used description for the rough wall profile is

$$u^+ = \frac{1}{k} \ln(y/k_s) + B \quad (39)$$

where B is a function of $Re_{(k)}$. Figure 48 shows the variations of B with $Re_{(k)}$ for sand-grain roughness (Nikuradse, 1950) and for the deterministic surface used in the Stanford program. The asymptotic value for fully rough behavior is the same for both surfaces--the difference lies in the transitional range. There is an abrupt change in B for the deterministic surface and a gradual change for the sand-grain roughness. This is believed to reflect the fact that there is a range of sizes of particles in the sand-grain

surface, and a range of geometries, while the deterministic roughness is "all one kind".

Discrete-hole injection raises an entirely new set of modeling problems, since the real flow is grossly three-dimensional. The approach followed at Stanford has been to reduce the three-dimensional problem to a two-dimensional one by spanwise averaging, and then to define the mixing length and turbulent Prandtl numbers based upon the spanwise averages.

Figures 49 and 50 show mean velocity and mean temperature profiles at several spanwise locations across the test plate, within the full-coverage region. When the velocity profiles are averaged, one can apply momentum conservation and the definition of mixing length to the averaged profiles and deduce an apparent distribution of the mixing length, l . The outcome of such an exercise is shown in Fig. 51. The peak in deduced mixing length reflects the augmented turbulent mixing caused by the injected jets. An idealized model of these results is shown in Fig. 52. The location and magnitude of the peak in mixing length are the two parameters which must be extracted from data to allow prediction of the results for different values of the injection parameter, M , and different injection geometries.

The models described above, for mixing length and turbulent Prandtl number, can be put into the STAN5 computer program and will permit predictions to be made of the heat transfer under combinations of conditions never actually tested. To test the validity of these predictions, it is necessary to compare predictions with measurements for those situations where data do exist.

In the last four figures, predictions and measurements will be compared to demonstrate the extent to which agreement has been established. Not all of the tested cases are shown here--for example, acceleration on a flat plate is well predicted by these models, but not shown here. Modeling of convex and concave flows and of mixed convection has not progressed to the same level as for the simpler cases, and will not be treated here.

Figure 53 shows measured and predicted values for Stanton number as a function of the enthalpy-thickness Reynolds number, using data from two programs reported here. These data describe a flat, smooth plate in a constant-velocity flow, with the wall at uniform temperature.

Figure 54 shows a comparison of measured and predicted Stanton numbers and friction factors for a smooth-wall flow subject to a mild deceleration, with and without transpiration through the wall. Except for the initial data point on each curve, the agreement is excellent.

Rough-wall predictions are shown in Fig. 55, compared with data with and without blowing through the rough surface. The conditions represented here are in the "fully rough" domain.

The last figure, Fig. 56, shows the predicted and measured Stanton numbers for discrete-hole injection (30° slant angle) using the augmented mixing-length model described earlier.

Conclusions

The accuracy of our ability to predict heat transfer depends on the breadth and accuracy of the data on which the modeling programs are based. At present, the smooth-wall and rough-wall situations seem in relatively good order, including the effects of streamwise acceleration and deceleration, as well as transpiration. Modeling of discrete-hole injection is still in its infancy, but results to date indicate that even the mixing-length approach can be made to work well. Thus it appears certain that some form of 2-D modeling will be devised.

Acknowledgments

The Stanford data reported here have been developed over a 25-year period under support from several different agencies: NSF, NASA, ONR, and AFOSR, in particular. The work presented here represents portions of the contributions of 22 doctoral and 2 engineer's degree programs.

Nomenclature

- α Thermal diffusivity.
- A^+ Damping factor for mixing length, Eqn. (14).
- A_R^+ Damping factor for mixing length on a rough wall, Eq. (34).
- B_f Blowing parameter based on friction, $\dot{m}''/(G C_f/2)$.
- B_h Blowing parameter based on heat transfer, $\dot{m}''/G St$.
- β Pressure gradient parameter, $\frac{\delta_1}{\tau_0} \frac{dp}{dx}$
- c_p Specific heat at constant pressure.
- $C_f/2$ Friction coefficient.
- ϵ Location of a step in wall temperature, Eqn. (16).
- ϵ_H Eddy diffusivity for heat.
- ϵ_M Eddy diffusivity for momentum.
- Δ_2 Enthalpy thickness, $\int_0^\infty \frac{\rho U}{\rho_\infty U_\infty} \left(\frac{t - t_\infty}{t_0 - t_\infty} \right) dy$.
- δ Boundary layer thickness to $u/u_\infty = 0.99$.
- δ_1 Displacement thickness, $\int_0^\infty \left(1 - \frac{\rho U}{\rho_\infty U_\infty} \right) dy$.
- δ_2 Momentum thickness, $\int_0^\infty \frac{\rho U}{\rho_\infty U_\infty} \left(1 - \frac{\rho U}{\rho_\infty U_\infty} \right) dy$.
- F Blowing fraction, $F = \dot{m}''/G$.
- g_c Proportionality constant, mass/force.
- G Free-stream mass velocity, $\rho_\infty U_\infty$.
- H Shape factor, δ_1/δ_2 .
- κ Mixing-length constant, $\kappa = 0.41$.
- k_s Equivalent sand-grain roughness.
- K Acceleration parameter, $\frac{v}{U_\infty^2} \frac{dU_\infty}{dx}$.
- K_R Acceleration parameter for a rough wall, $\frac{r}{U_\infty} \frac{dU_\infty}{dx}$.

l	Mixing length, Eqn. (3).
m	Acceleration parameter used in Eqn. (11).
\dot{m}''	Mass flux injected through the surface.
ν	Kinematic viscosity.
p	Pressure.
Pr	Prandtl number.
Pr_T	Turbulent Prandtl number.
dp/dx	Pressure gradient in the streamwise direction.
p^+	Pressure gradient parameter, $\frac{\nu}{\rho U_\tau^3} \frac{dp}{dx}$.
ρ_0	Density of injectant.
ρ_∞	Density of free stream fluid.
T_0	Temperature of the wall.
T_∞	Temperature of the free stream.
τ_0	Wall shear stress.
U_∞	Velocity of free stream.
u, U	Velocity in the x-direction.
u_τ	Friction velocity, $\sqrt{g_c \tau_0 / \rho}$.
v, V	Velocity in the y-direction.
v_0	Velocity of injectant.
v_0^+	Blowing parameter, v_0 / u_τ .
ν	Kinematic viscosity.
Re_k	Roughness Reynolds number, $u_\tau k_s / \nu$.
Re_k	Roughness Reynolds number for onset of fully rough flow, Eqn. (32).
Re_x	x-Reynolds number, $U_\infty x / \nu$.
Re_{Δ_2}	Enthalpy thickness Reynolds number, $U_\infty \Delta_2 / \nu$.
Re_{δ_2}	Momentum thickness Reynolds number, $U_\infty \delta_2 / \nu$.
ψ	$\frac{1}{4}$ constant in Eqn. (33).

REFERENCES

- Blackwell, B. P., Kays, W. M., and Moffat, R. J. (1972), "The Turbulent Boundary Layer on a Porous Plate: An Experimental Study of the Heat-Transfer Behavior with Adverse Pressure Gradients," Stanford University Thermosciences Division Report HMT-16.
- Bradshaw, P., and Simonich, P. (1978) "Effect of Free-Stream Turbulence on Heat Transfer through a Turbulent Boundary Layers," J. of Heat Trans., 100, No. 4, 1978.
- Brown, A., and Burton, R. C. (1978), "The Effects of Free-Stream Turbulence Intensity and Velocity Distribution on Heat Transfer to Curved Surfaces," Jour. of Engrg. for Power, Vol. 100, 1978, pp. 159-168.
- Brown, A., and Martin, B. W. (1979), "Heat Transfer to Turbine Blades, with Special Reference to the Effects of Mainstream Turbulence," ASME Preprint 79-GT-26, March 1979.
- Choe, H., Kays, W. M., and Moffat, R. J. (1975), "The Turbulent Boundary Layer on a Full-Coverage Film-Cooled Surface: An Experimental Heat Transfer Study with Normal Injection," Stanford University Thermosciences Division Report HMT-22.
- Coleman, H. W., Moffat, R. J., and Kays, W. M. (1976), "Momentum and Energy Transport in the Accelerated, Fully Rough, Turbulent Boundary Layer," Stanford University Thermosciences Division Report HMT-24.
- Consigny, H., Ehan, C. K., and Richards, B. E., "The Effect of Pressure Gradient and External Turbulence on Heat Transfer to a Cold, Flat Plate," VKI TN 128, February 1979.
- Crawford, M. E., Kays, W. M., and Moffat, R. J. (1976), "Heat Transfer to a Full-Coverage Film-Cooled Surface with 30° Slant-Hole Injection," NASA CR-2786, Dec. 1976.
- Crawford, M. E., and Kays, W. M. (1976), "STAN5--A Program for Numerical Computation of Two-Dimensional Internal and External Boundary Layer Flows," NASA CR-2742, 1976.
- Favre, A., Dumas, R., Verollet, E., and Gantic, M. (1966), "Couche Limite Turbulente sur Paroi Poreuse avec Aspiration," Jour. de Mechanique, Vol. 5, No. 1, p. 4, 1966.
- Feller, C. E., "Experimental Heat Transfer and Boundary Layer Behavior with 100 cps Flow Oscillations," NASA TN-D2521 (1964).
- Georgieu, D. P., Godard, M., and Richards, B. E., "Experimental Study of the Iso-Heat-Transfer-Rate Lines on the End Wall of a Turbine Cascade," ASME Preprint 79-GT-20.
- Gillis, J. C., Johnston, J. P., Kays, W. M., and Moffat, R. J. (1980), "Turbulent Boundary Layer on a Convex, Curved Surface," Stanford University Thermosciences Division Report HMT-31, 1980.

- Healzer, J. M. (1974), "The Turbulent Boundary Layer on a Rough, Porous Plate: Experimental Heat Transfer with Uniform Blowing," Ph.D. thesis, Stanford University; see also Thermosciences Division Report HMT-18.
- Joselevich, V. A., and Pilipenko, V. J. (1974), "Logarithmic Velocity Profile for Flow of a Weak Polymer Solution near a Rough Surface," Sov. Phys. Dokl., Vol. 18, p. 790.
- Julien, H., Kays, W. M., and Moffat, R. J. (1969), "The Turbulent Boundary Layer on a Porous Plate: Experimental Study of the Effects of a Favorable Pressure Gradient," Stanford University Thermosciences Division Report HMT-4.
- Kays, W. M., and Crawford, M. E., Convective Heat and Mass Transfer, McGraw-Hill Book Co., 1980.
- Kays, W. M., and Moffat, R. J. (1975), in Studies in Convection, Vol. 1, Academic Press, pp. 213-319.
- Kearney, D. W., Kays, W. M., and Moffat, R. J. (1970), "The Effect of Free-stream Turbulence on Heat Transfer to a Strongly Accelerated Turbulent Boundary Layer," Proceedings of the 1970 Heat Transfer and Fluid Mechanics Institute, edited by T. Sarpkaya (Stanford University Press), pp. 3-14.
- Kendall, R. M. (1959), "Interaction of Mass and Momentum Transfer in the Turbulent Boundary Layer," Sc.D. thesis, M.I.T.
- Kestin, J. (1966), "The Effect of Free-Stream Turbulence on Heat Transfer Rates," Advances in Heat Transfer, pp. 31-32.
- Kim, H. K., Moffat, R. J., and Kays, W. M. (1979), "Heat Transfer to a Full-Coverage, Film-Cooled Surface with Compound-Angle (30° and 45°) Injection," NASA CR-3103, Feb. 1979.
- Ligrani, P. M. (1979), "The Thermal and Hydrodynamic Behavior of Thick, Rough-Wall, Turbulent Boundary Layers," Ph.D. thesis, Stanford University.
- Mayle, R. E., Blair, M. F., and Kopper, F. C. (1979), "Turbulent Boundary Layer Heat Transfer on Curved Surfaces," Jour. of Heat Trans., Vol. 101, No. 3, 1979.
- Mickley, H. S., Ross, R. C., Squyers, A. L., and Stewart, W. E. (1954), "Heat, Mass, and Momentum Transfer for Flow over a Flat Plate with Blowing or Suction," NACA TN-3208, 1954.
- Mickley, H. S., and Davis, R. S. (1957), "Momentum Transfer for Flow over a Flat Plate with Blowing," NACA TN-4017, 1957.
- Moffat, R. J. (1967), "The Turbulent Boundary Layer on a Porous Plate: Experimental Heat Transfer with Uniform Blowing and Suction," Ph.D. thesis, Stanford University.

- Moffat, R. J., Healzer, J. M., and Kays, W. M. (1978), "Experimental Heat Transfer Behavior of a Turbulent Boundary Layer on a Rough Surface with Blowing," ASME Jour. of Heat Transfer, Vol. 100, p. 134, Feb. 1978.
- Monin, A. S., and Yaglom, A. M. (1971), Statistical Fluid Mechanics, Vol. 1, The MIT Press.
- Moretti, P. M. (1964), "Heat Transfer Through an Incompressible Turbulent Boundary Layer with Varying Free-Stream Velocity and Varying Surface Temperature," Ph.D. thesis, Stanford University. Also Dept. of Mech. Engrg. Report PG-1.
- Nikuradse, J. (1950), "Stromungsgestze in rauhen Rohren," VDI Forschungshaft, No. 361, English translation. NACA TM-1292.
- Orlando, A. F., Moffat, R. J., and Kays, W. M. (1974), "Turbulent Transport of Heat and Momentum in a Boundary Layer Subject to Deceleration, Suction, and Variable Wall Temperature," Stanford University Thermosciences Division Report HMT-17.
- Perry, A. E., and Joubert, P. H. (1963), "Rough Wall Boundary Layers in Adverse Pressure Gradients," J. Fluid Mech., 37, pp. 163-211.
- Pimenta, M. M., Moffat, R. J., and Kays, W. M. (1979), "The Structure of a Boundary Layer on a Rough Wall with Blowing and Heat Transfer," ASME Jour. of Heat Transfer, Series C, Vol. 101, 1979.
- Reynolds, W. C., Kays, W. M., and Kline, S. J. (1958a), "Heat Transfer in the Turbulent, Incompressible Boundary Layer," NASA Memo 12-1-58W.
- Reynolds, W. C., Kays, W. M., and Kline, S. J. (1958b), "Heat Transfer in the Turbulent Incompressible Boundary Layer. II. Step-Wall Temperature Distribution," NASA Memorandum 12-2-58W.
- Reynolds, W. C., Kays, W. M., and Kline, S. J. (1958c), "Heat Transfer in the Turbulent Incompressible Boundary Layer. III. Arbitrary Wall Temperature and Heat Flux," NASA Memorandum 12-3-58W.
- Reynolds, W. C., Kays, W. M., and Kline, S. J. (1958d), "Heat Transfer in the Turbulent Incompressible Boundary Layer. IV. Effect of Location of Transition and Prediction of Heat Transfer in a Known Transition Region," NASA Memorandum 12-4-58W
- Schlichting, H. (1968), Boundary Layer Theory, 6th edition, McGraw-Hill, p. 586.
- Siebers, D. L., Schwind, R. G., and Moffat, R. J. (1983), "Experimental Mixed Convection Heat Transfer from a Large, Vertical Surface in a Horizontal Flow," Stanford University Thermosciences Division Report HMT-36.
- Slanciauskas, A., and Pedesius, A. (1977), "Effect of Free-Stream Turbulence on the Heat Transfer in the Turbulent Boundary Layer," Paper FC(1)-5, Academy of Sciences of the Lithuanian SSR Institute of Physical and Technical Problems of Energetics, Kaunos, USSR.

- Thomann, H. (1967), "Heat Transfer in a Turbulent Boundary Layer with a Pressure Gradient Normal to the Flow," Aero Res. Inst. of Sweden, Report No. 113.
- Torii, K., Nishiwaki, N., and Hirata, M. (1966), "Heat Transfer and Skin Friction in Turbulent Boundary Layer (sic) with Mass Injection," Proc. 3rd Int. Ht. Trans. Conf., AIChE and ASME, 1966.
- van Driest, E. R. (1956), "On Turbulent Flow Near a Wall," Heat Transfer and Fluid Mechanics Institute.
- Whitten, D. G., Kays, W. M., and Moffat, R. J. (1967), "The Turbulent Boundary Layer on a Porous Plate: Experimental Heat Transfer with Variable Suction, Blowing, and Surface Temperature," Stanford University Thermosciences Division Report HMT-3.
- Yen, K. T. (1977), "Experimental Heat Transfer in a Tube with a Pulsating Turbulent Flow," Engineer's Degree thesis, Dept. of Mech. Engrg., Stanford University.

FACTORS AFFECTING THE HEAT TRANSFER COEFFICIENT

REYNOLDS NUMBER, MACH NUMBER, GEOMETRY

PLUS

WALL TEMPERATURE	TRANSPIRATION
ACCELERATION	DISCRETE INJECTION
DECELERATION	SURFACE CURVATURE
TURBULENCE	UNSTEADINESS
ROUGHNESS	SECONDARY FLOW

Fig. 1. A list of important factors affecting heat transfer on blades and vanes of gas turbines.

X-MOMENTUM DIFFERENTIAL EQUATION

$$U \frac{\partial U}{\partial x} + v \frac{\partial U}{\partial y} - \frac{\partial}{\partial y} (\epsilon_M + \nu) \frac{\partial U}{\partial y} = - g_c \frac{dp}{dx} \quad \frac{\partial U}{\partial x} + \frac{\partial v}{\partial y} = 0$$

WITH: $\epsilon_M, \nu, \frac{dp}{dx}, U(x,0), U(x,\Delta), U(0,y)$

YIELDS:

$$\frac{C_f}{2} = \frac{C_f}{2} \{ \text{DOMAIN, VEL. DIST., FLU. PRO., VBC, VIC} \}$$

TURBULENCE CLOSURE

PRANDTL MIXING LENGTH: $\epsilon_M = \lambda^2 \left| \frac{\partial U}{\partial y} \right|$

$$\lambda = 0.41 y \left[1 - \exp \left\{ - y^+ / A^+ \right\} \right]$$

$$A^+ = f \{ v_0^+, p^+, \text{roughness, curvature} \}$$

Fig. 2. A representative differential equation and boundary conditions for x-momentum.

ENERGY DIFFERENTIAL EQUATION

$$U \frac{\partial T}{\partial x} + V \frac{\partial T}{\partial y} - \frac{\partial}{\partial y} (\epsilon_H + \alpha) \frac{\partial T}{\partial y} = 0$$

WITH: $U, V, \epsilon_H, \alpha, T(x,0), T(x,\Delta), T(0,y)$

YIELD: $ST = ST \{ \text{DOMAIN, VEL. DIST., FLU. PRO., TBC, TIC} \}$

TURBULENCE CLOSURE

$$\text{TURBULENT PRANDTL NO.: } \epsilon_H \triangleq \frac{c_M}{PR_T}$$

$$PR_T = F \{ Y^+, V_0^+, P^+, \text{ROUGHNESS, CURVATURE} \}$$

Fig. 3. A representative differential equation and boundary conditions for energy.

X-MOMENTUM INTEGRAL FORMS

$$\frac{c_f}{2} + \frac{\dot{m}''}{G} = \frac{d\delta_2}{dx} + \delta_2 \left[(2+H) \frac{1}{U_\infty} \frac{dU_\infty}{dx} \right]$$

$$\frac{d}{dx} (U_\infty^2 \delta_2) = \frac{g_c T_0}{\rho_\infty} \left(1 + \frac{\dot{m}''}{G(c_f/2)} + \frac{\delta_1}{\tau_0} \frac{dp}{dx} \right)$$

$$\frac{d(\text{Re}_{\delta_2})}{\left(\frac{U_\infty dx}{\nu} \right)} = \frac{c_f}{2} + \frac{\dot{m}''}{G} - \frac{\nu}{U_\infty^2} \frac{dU_\infty}{dx} (1+H) \text{Re}_{\delta_2}$$

Fig. 4. The integral equation for x-momentum as a guide to experiments with variable boundary conditions.

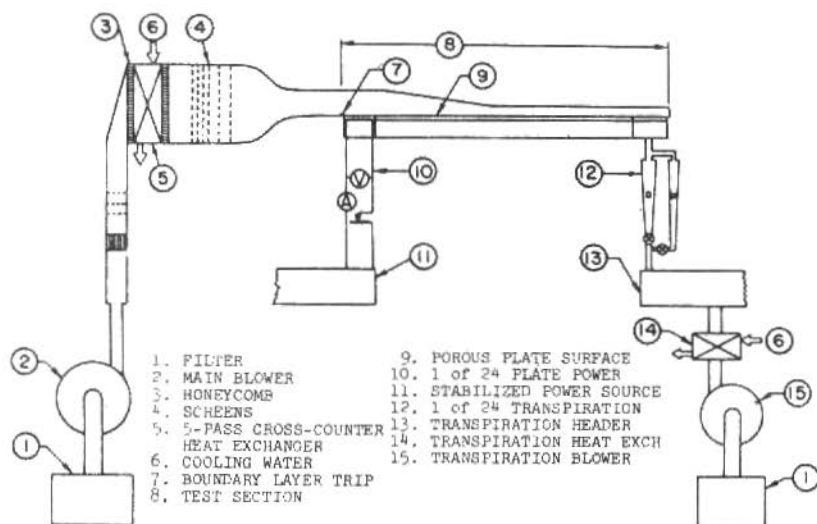


Fig. 5. Schematic of tunnel HMT-1, used for smooth-wall studies with transpiration, variable velocity and variable wall temperature

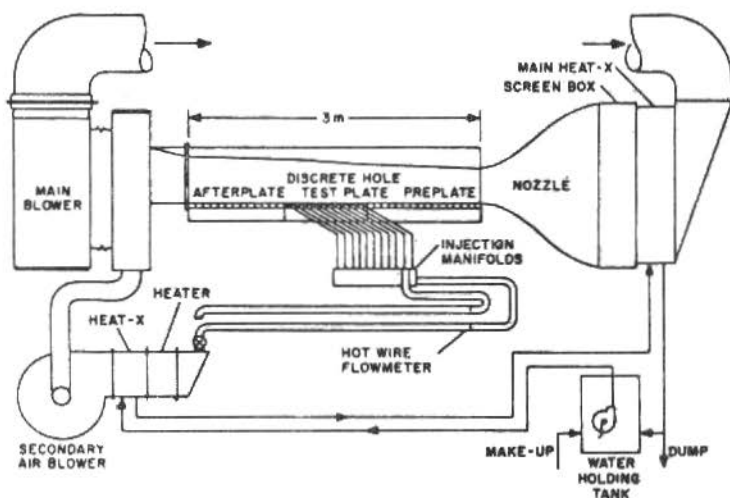


Fig. 6. Schematic typical of tunnels HMT-2 and HMT-3 used for rough-wall studies and for discrete-hole injection with various hole patterns.

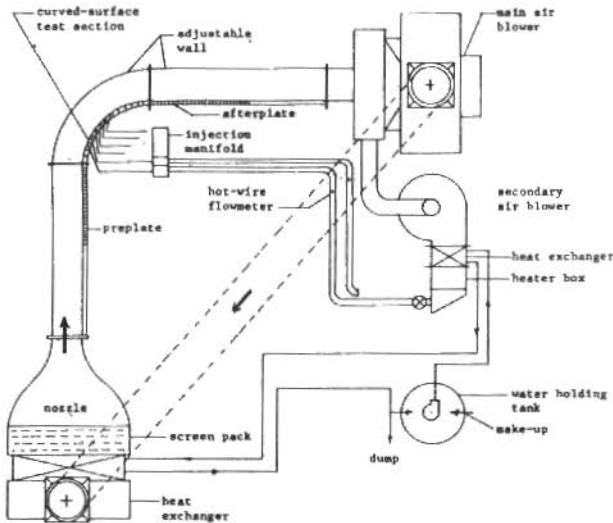


Fig. 7. Schematic of tunnel HMT-4, used for studies of curvature effects with and without discrete-hole injection.

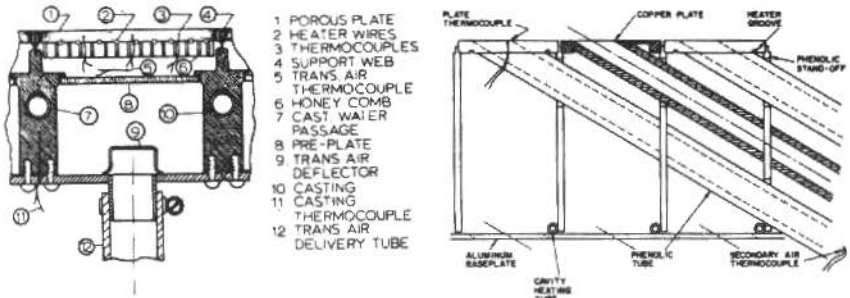


Fig. 8. Examples of test-plate construction for the porous plate (8a) and the discrete-hole (8b) test surfaces used in tunnels 1-4.

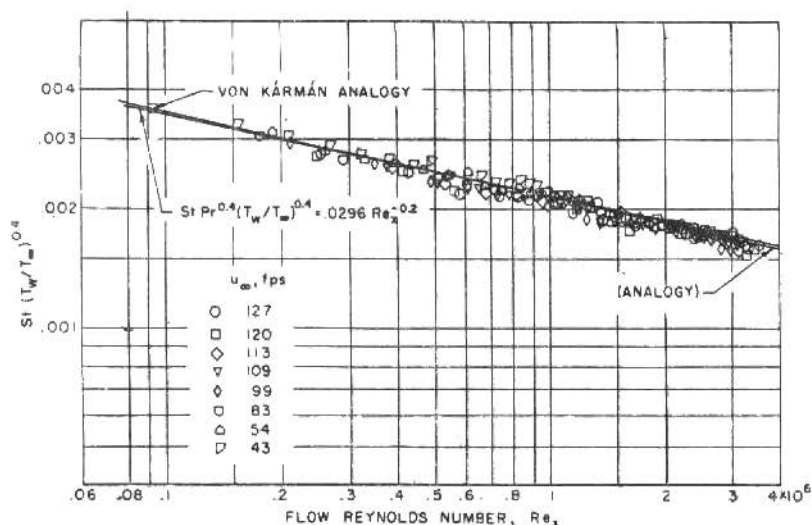


Fig. 9. Stanton number vs. x-Reynolds number for a smooth plate of uniform

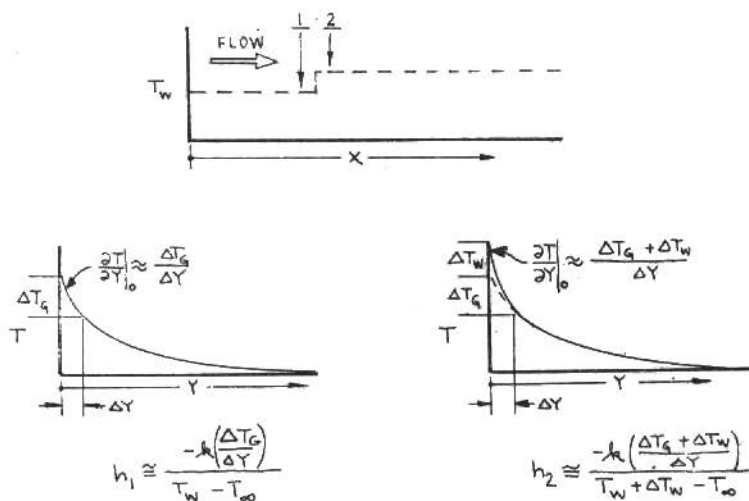


Fig. 10. A schematic representation of the means whereby steps in wall temperature affect the coefficient of heat transfer.

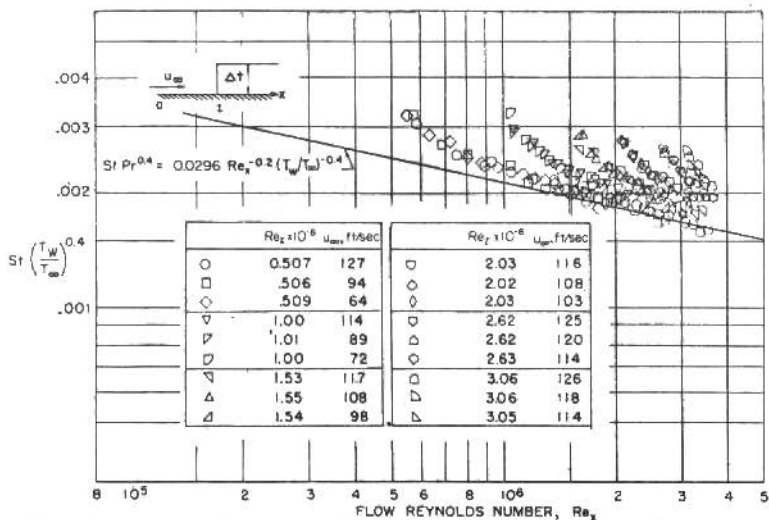


Fig. 11. Stanton number vs. x-Reynolds number for a smooth plate with a step in wall temperature at various positions (Reynolds et al., 1958b).

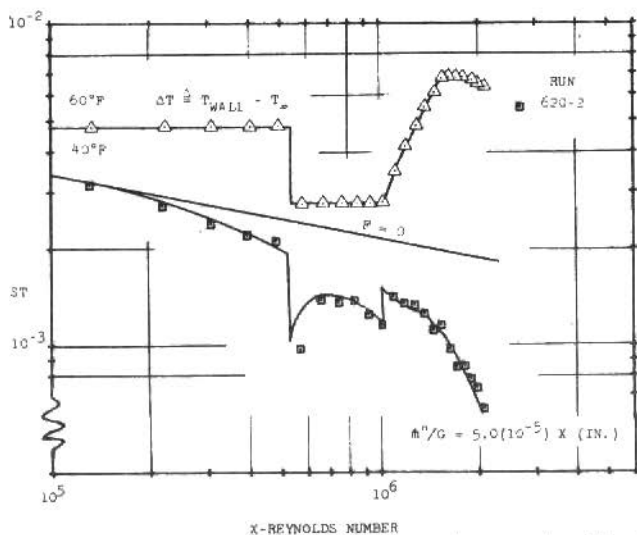


Fig. 12. Example of combined effects of linearly varying blowing and an arbitrary variation of wall temperature (Whitten, 1967).

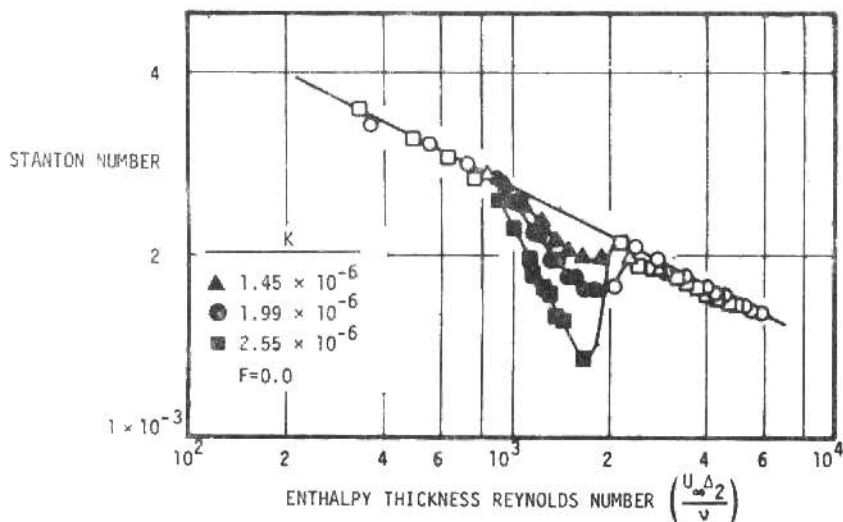


Fig. 13. Effects of moderate & strong acceleration on smooth-wall boundary layer; no transpiration, uniform wall temp. (Kays & Moffat, 1975).

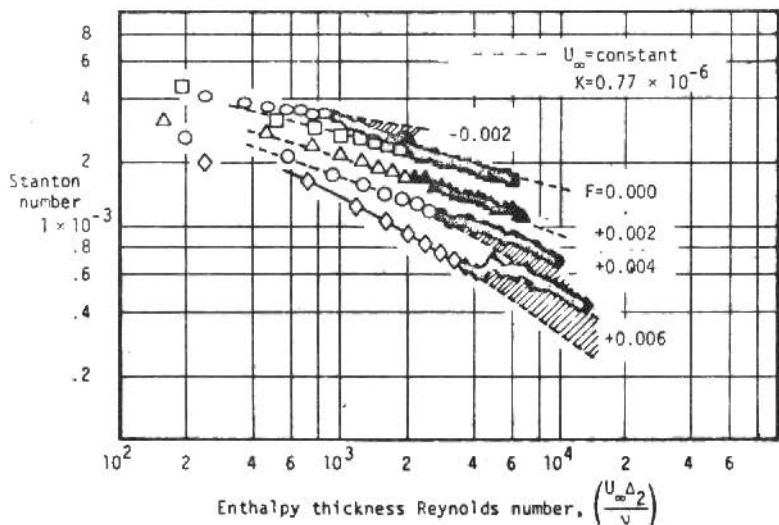


Fig. 14. Effects of moderate acceleration on smooth-wall boundary layer with transpiration, uniform F; uniform wall temp. (Kays & Moffat, 1975).

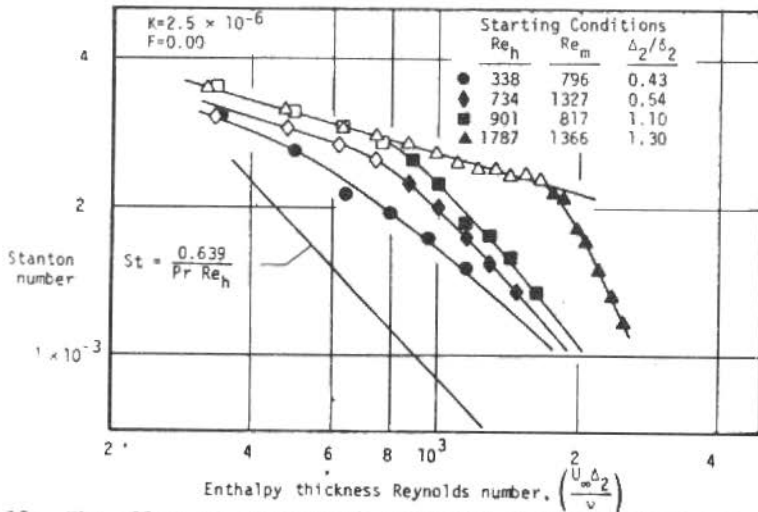


Fig. 15. The effect of the initial condition of the boundary layer on its response to strong acceleration (Kays & Moffat, 1975).

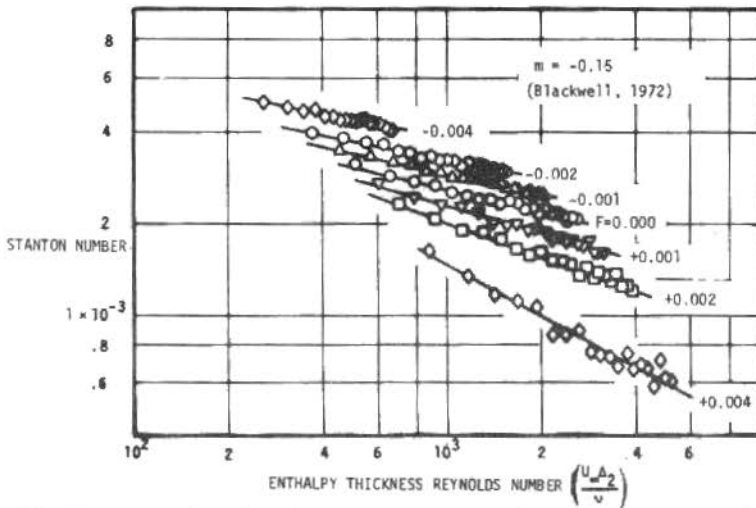


Fig. 16. Evidence that deceleration does not alter the relationship between Stanton number and enthalpy thickness Reynolds number.

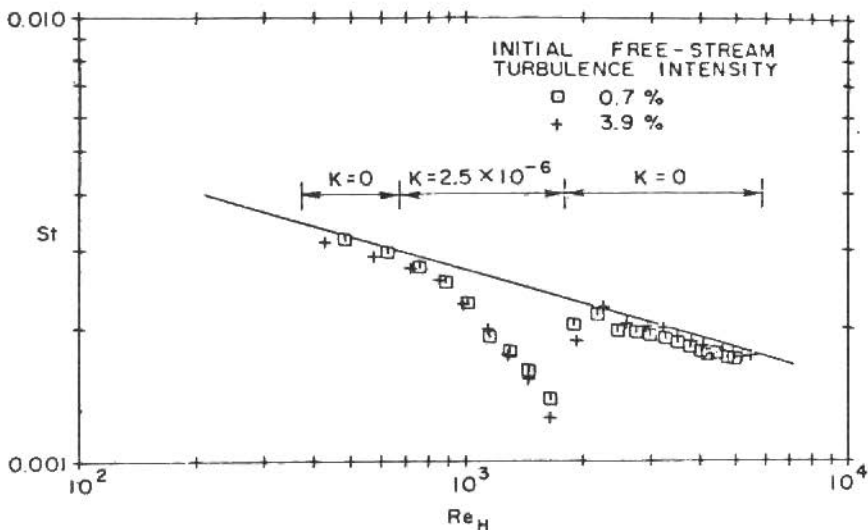


Fig. 17. Effect of free-stream turbulence on heat transfer through turbulent boundary layer with strong acceleration (Kearney et al., 1970)

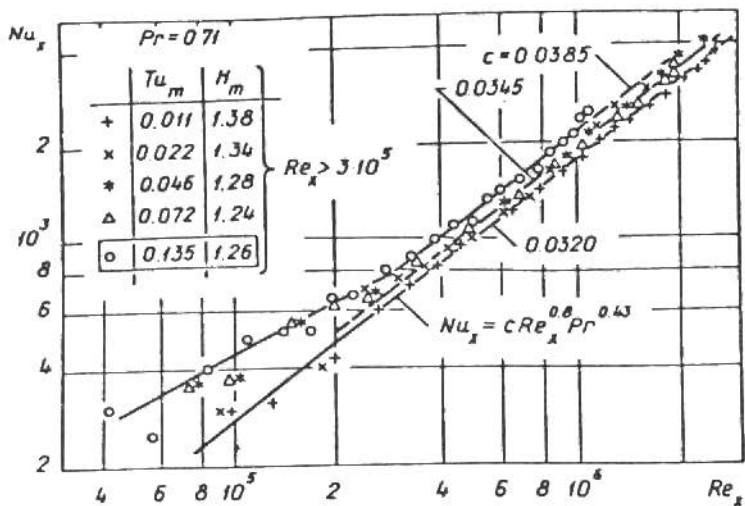


Fig. 18. The effect of free-stream turbulence on heat transfer with no pressure gradient (Slanciauskas & Pedesius, 1977).

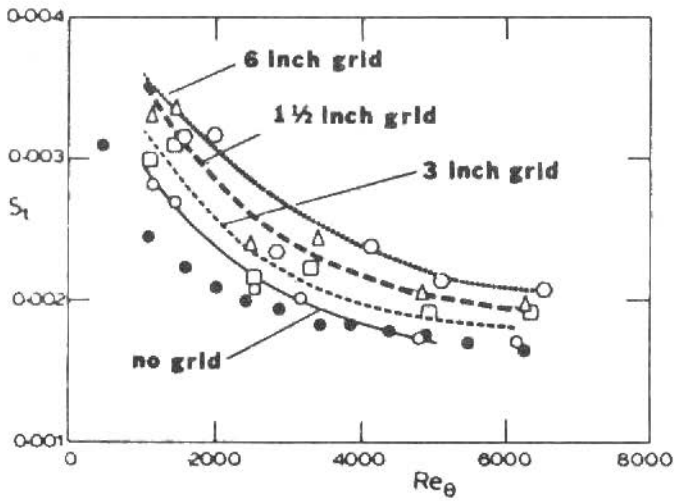


Fig. 19. Simonich and Bradshaw (1978) results concerning the effects of turbulence on heat transfer.

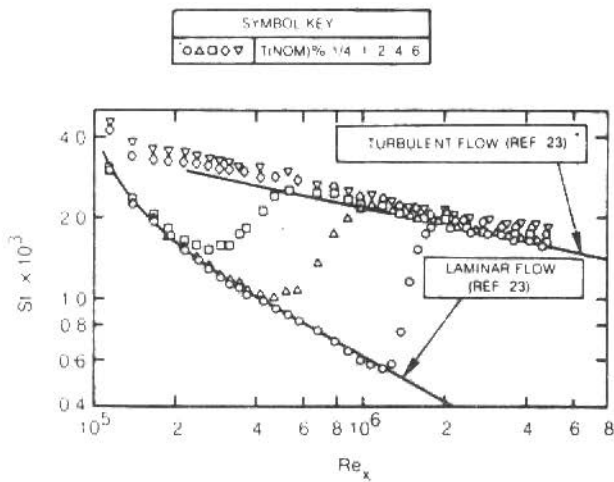


Fig. 20. The effect of free-stream turbulence on heat transfer (Blair, 1983).

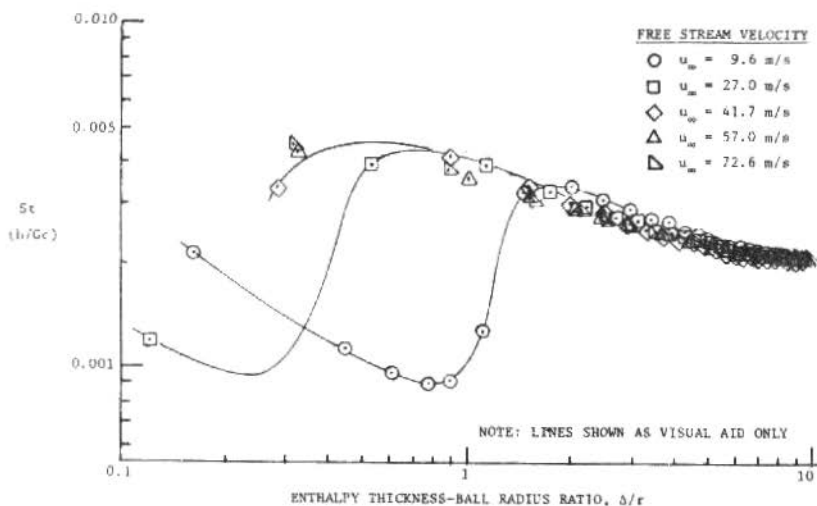


Fig. 21. Stanton number vs. enthalpy thickness: flow over a rough wall with no transpiration; uniform wall temp. (Moffat, 1978).

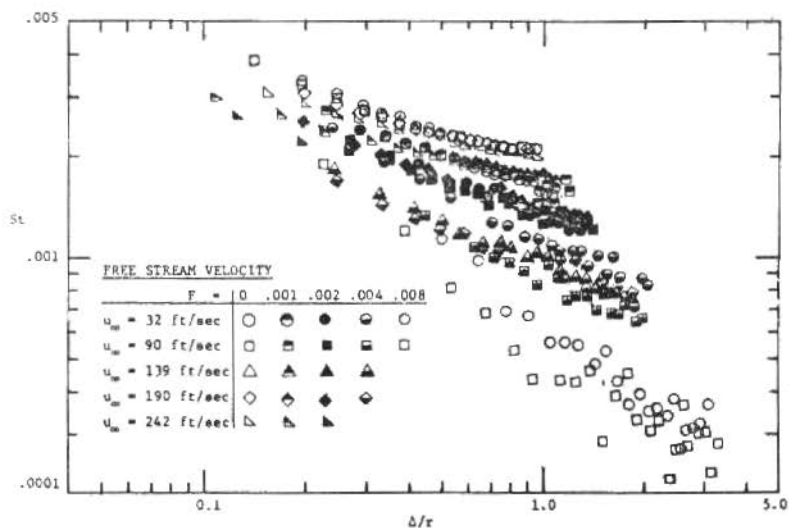


Fig. 22. Stanton number vs. enthalpy thickness: flow over a rough wall with transpiration, uniform wall temp. (Moffat, 1978).

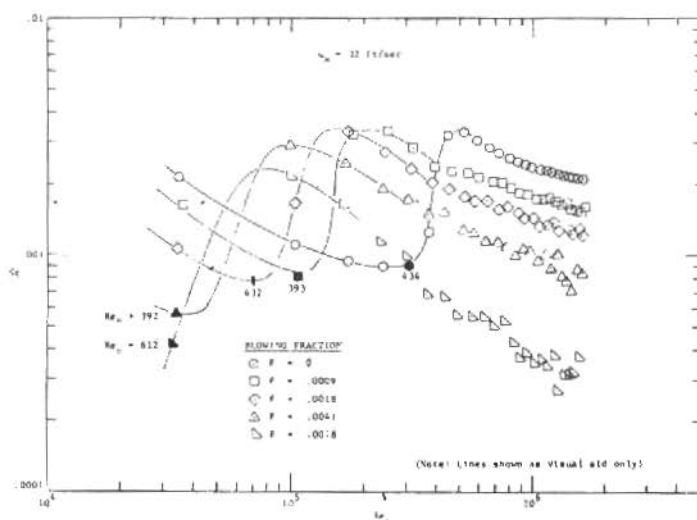


Fig. 23. Transition behavior of a rough surface with blowing (Moffat, 1978).

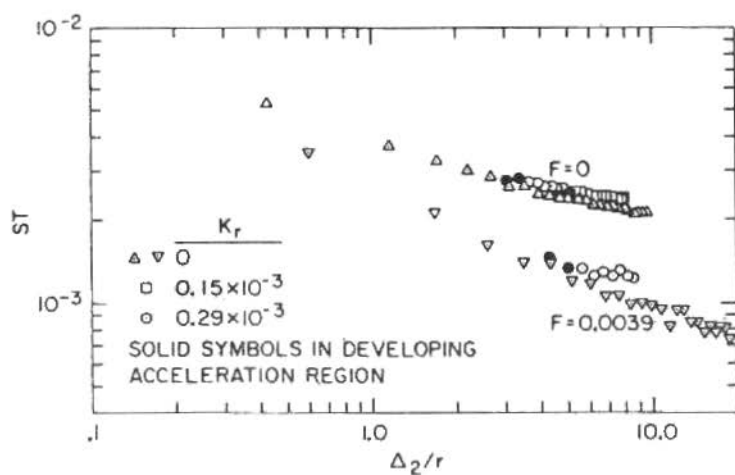


Fig. 24. Acceleration effects on a rough wall boundary layer with blowing (Coleman, 1976).

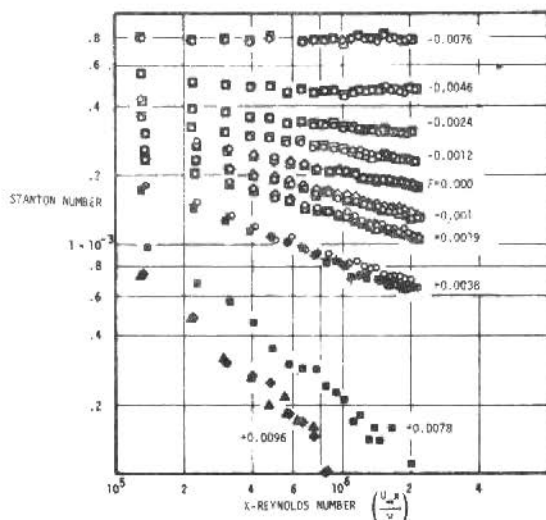


Fig. 25. Stanton number vs. x-Reynolds number for transpiration through a smooth plate of uniform wall temperature (Moffat & Kays, 1968).

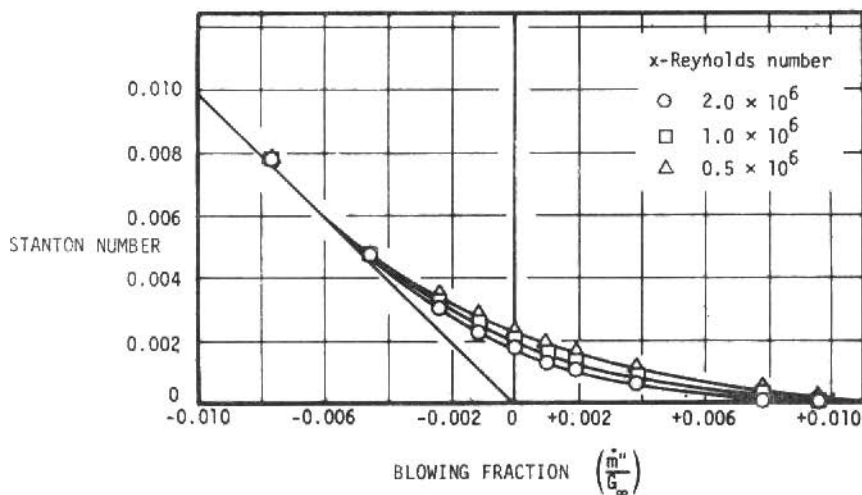


Fig. 26. Stanton number vs. blowing fraction, m''/G , parametric in x-Reynolds number (Moffat & Kays, 1968).

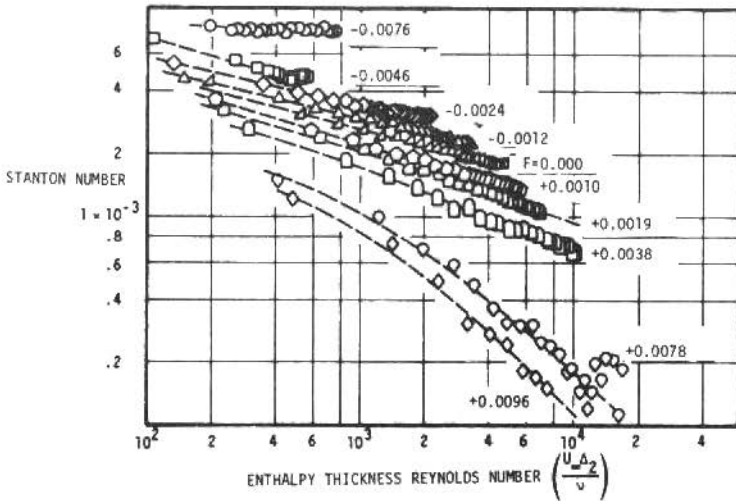


Fig. 27. Stanton number vs. enthalpy thickness Reynolds number for transpiration through a smooth plate of uniform temp. (Moffat, 1967).

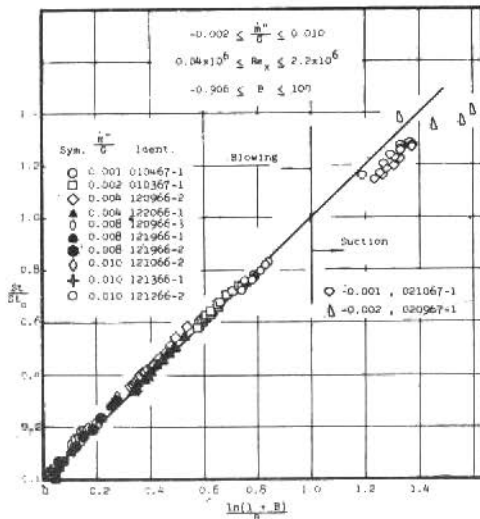


Fig. 28. Ratio of measured St with blowing to St without, at same x -Reynolds No., compared to Couette flow $\ln(1+B)/B$ (Moffat, 1967).

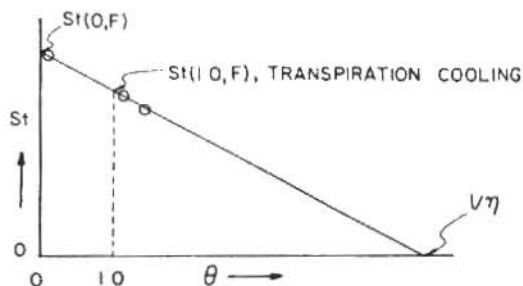


Fig. 29. Illustration of the superposition theorem and its relationship to the concept of adiabatic wall effectiveness.

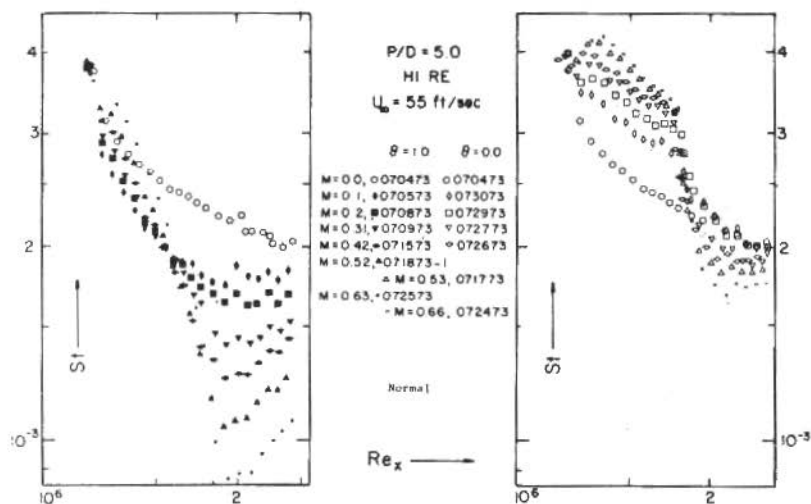


Fig. 30. Stanton number, vs. x -Reynolds No., normal injection. Data for $\theta = 0.0$ and $\theta = 1.00$ for M between 0.0 & 0.63 (Crawford et al., 1975).

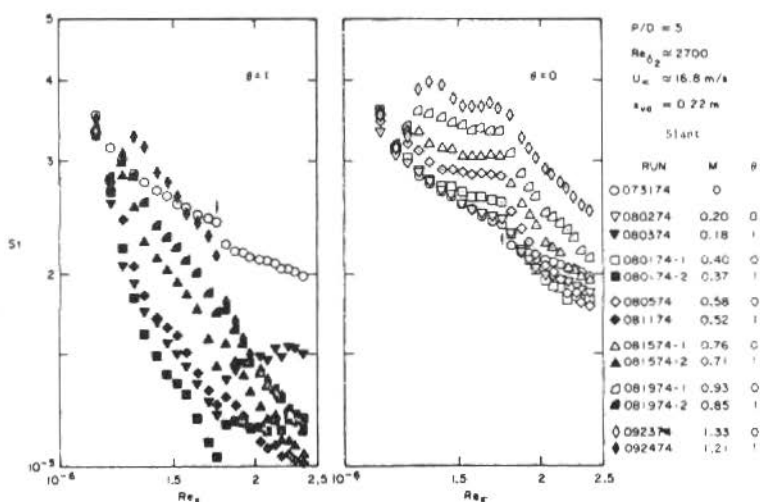


Fig. 31. Stanton no. vs. x-Reynolds no. for 30° slant-hole injection; $\theta = 0.0$ and $\theta = 1.00$, unheated starting length (Crawford et al., 1975).

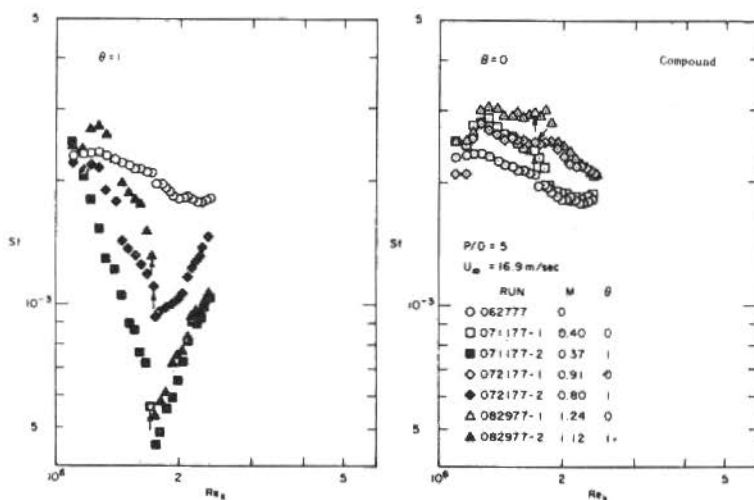


Fig. 32. Stanton no. vs. x-Reynolds no., compound-angle injection (30° slant, 45° skew), $\theta = 0.0$ & 1.00 , heated starting length (Kim, 1978).

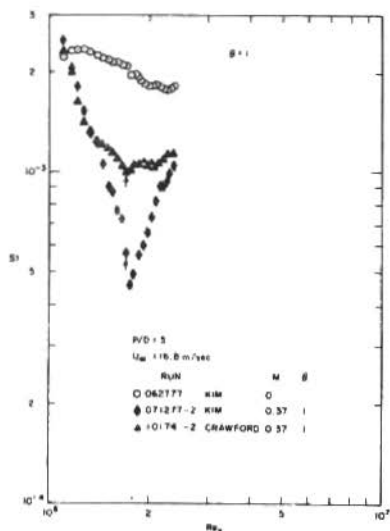


Fig. 33. Comparison of slant-angle and compound angle film cooling under otherwise comparable conditions (Kim et al., 1979).

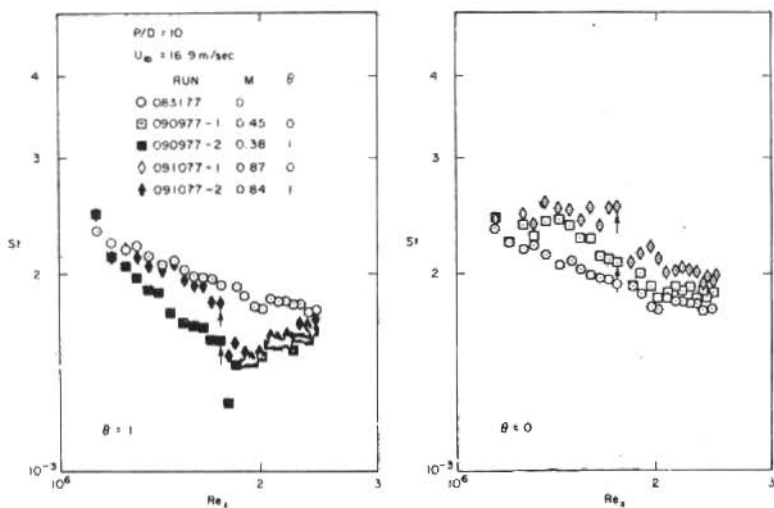


Fig. 34. Stanton number vs. x-Reynolds number for $P/D = 10.0$, heated starting length (Kim et al., 1979).

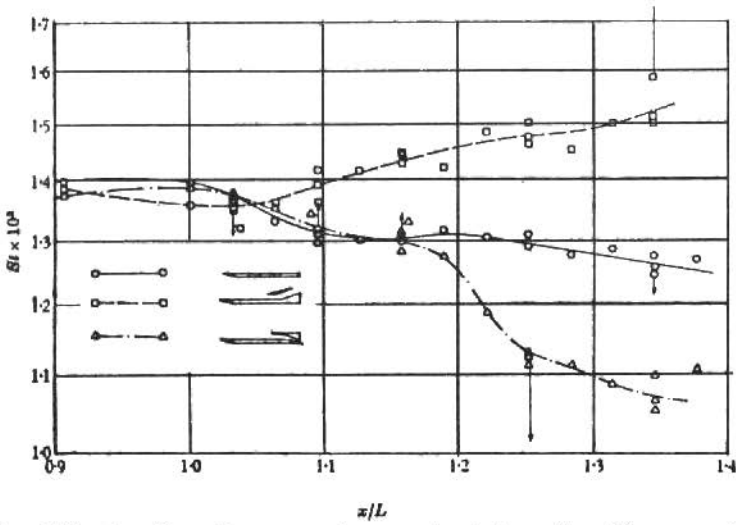


Fig. 35. Effects of surface curvature on heat transfer (Thomann, 1968).

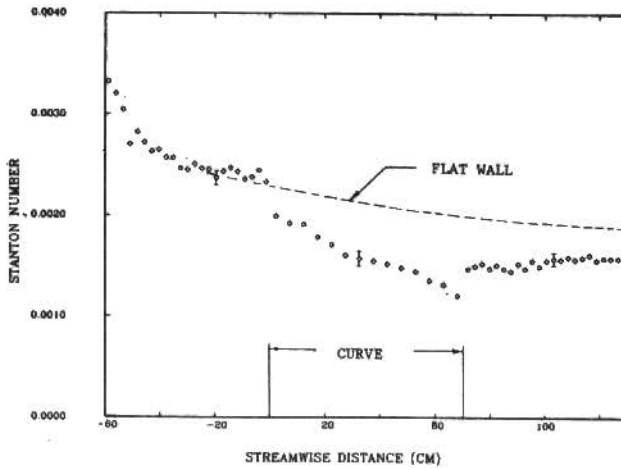


Fig. 36. The effect of strong convex curvature on heat transfer for $\delta_{0,55}/R = 0.10$, $U_{\infty} = 14.8$ m/s, $K = 0.0$ (Simon et al., 1980)

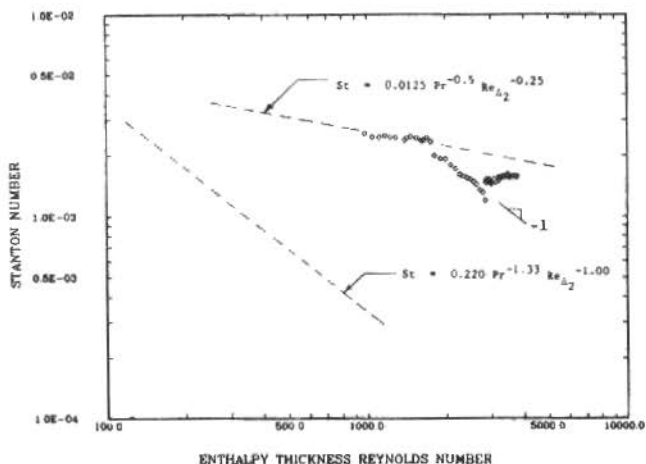


Fig. 37. The effect of strong convex curvature on heat transfer for $\delta_{0.99}/R = 0.10$, $U_\infty = 14.8$ m/s, $K = 0.0$ (Simon et al., 1980).

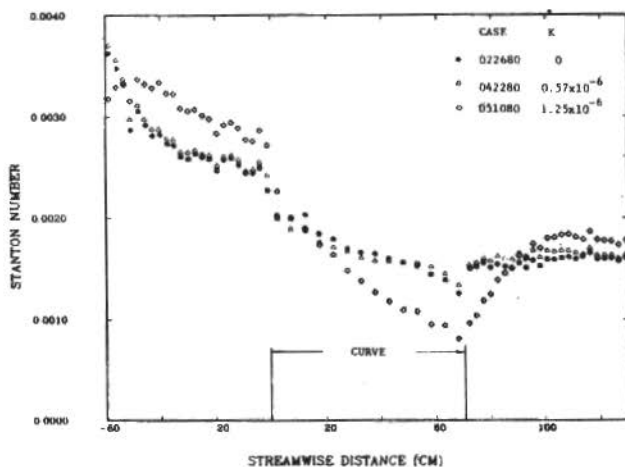


Fig. 38. The combined effects of acceleration and convex curvature on heat transfer (x -coordinates), $\delta_{0.99}/R = 0.5$ (Simon et al., 1980).

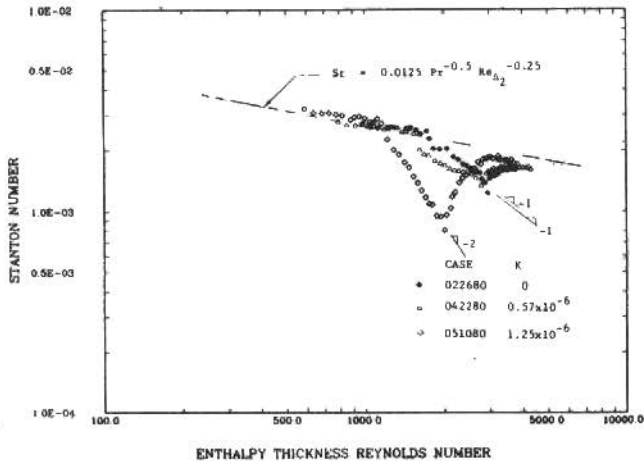


Fig. 39. The combined effects of acceleration and convex curvature on heat transfer (Re_{Δ_2} coordinates), for $\delta_{0.99}/R = 0.05$ (Simon et al., 1980).

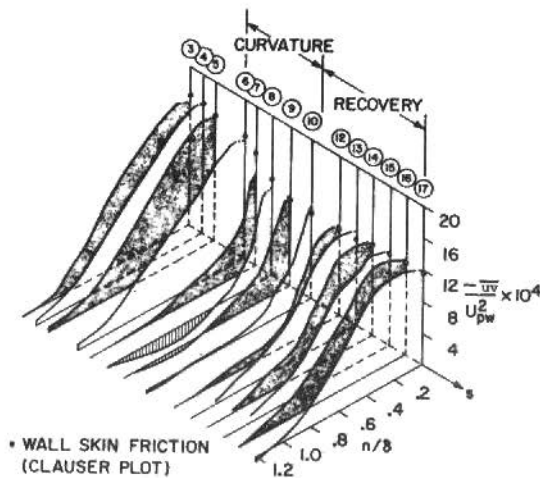


Fig. 40. Isometric view of shear stress distributions in a convex turbulent boundary layer (Gillis et al., 1980).

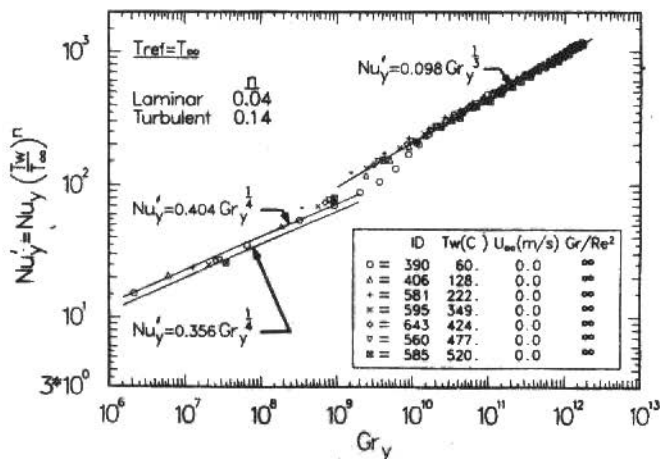


Fig. 41. Free convection heat transfer with a variable-properties correction (Siebers et al., 1983).

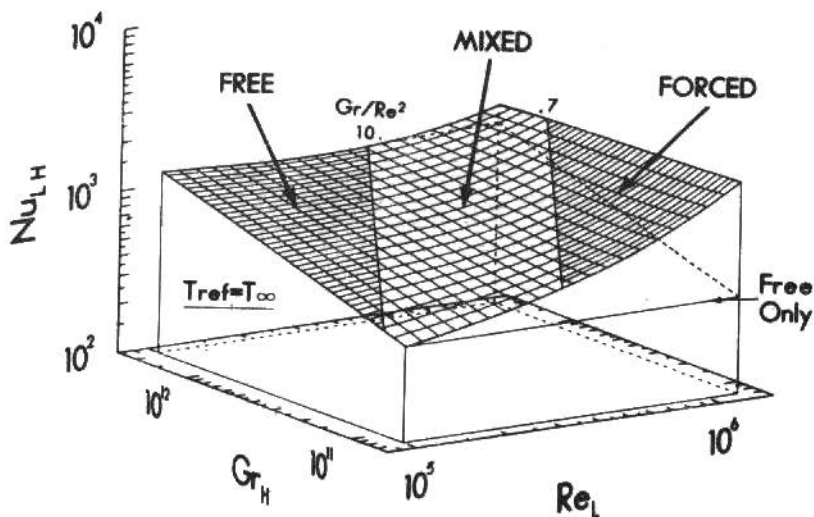


Fig. 42. Average heat transfer coefficient as a function of free-stream velocity and wall temperature (Siebers et al., 1983).

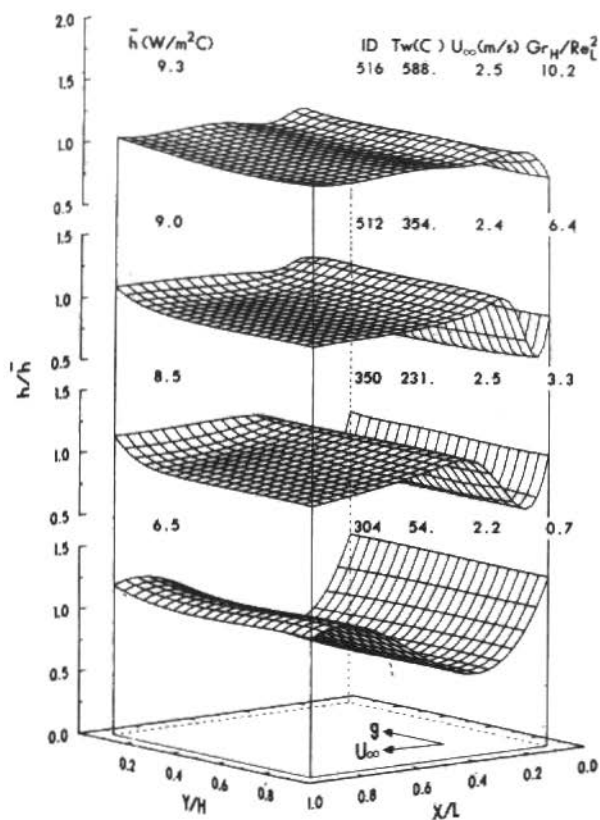


Fig. 44. Distribution of the heat-transfer coefficient over the surface-constant wall temperature and variable free-stream velocity (Siebers et al., 1983).

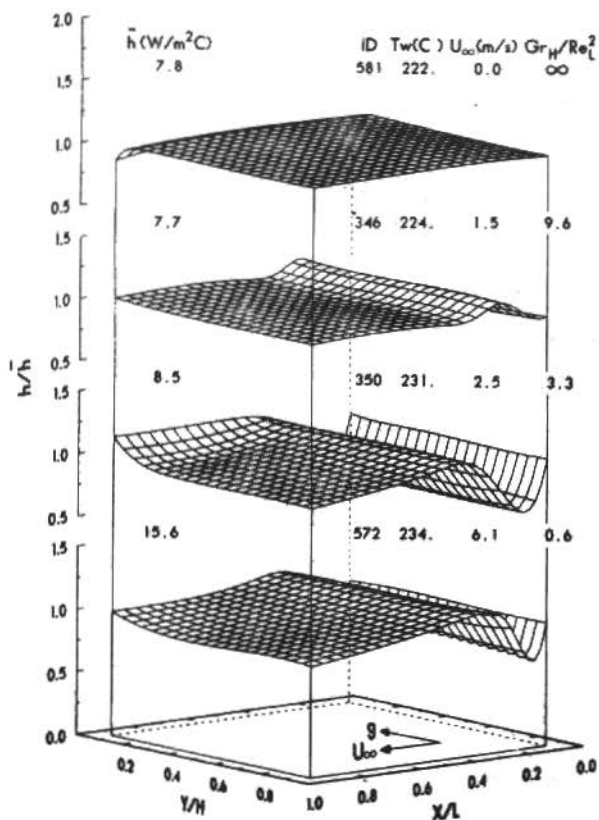


Fig. 43. Distribution of the heat-transfer coefficient over the surface-constant free-stream velocity, variable wall temperature (Siebers et al., 1983).

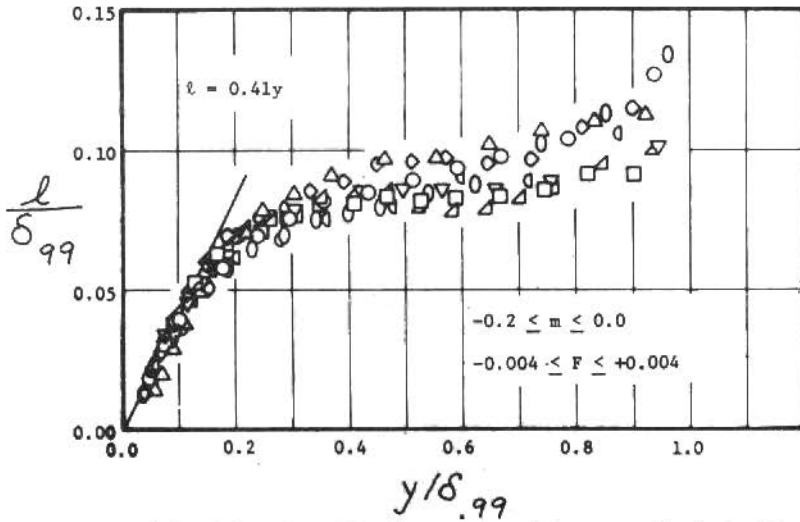


Fig. 45 Prandtl mixing-length values deduced for smooth-plate flows with deceleration and transpiration (Kays and Moffat, 1975).

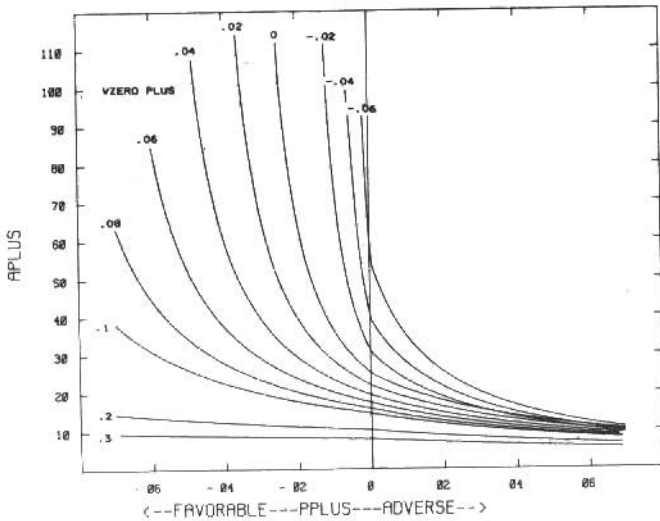


Fig. 46 Variation of A^+ with p^+ and v_0^+ used in the STANS program to account for pressure gradients and transpiration.

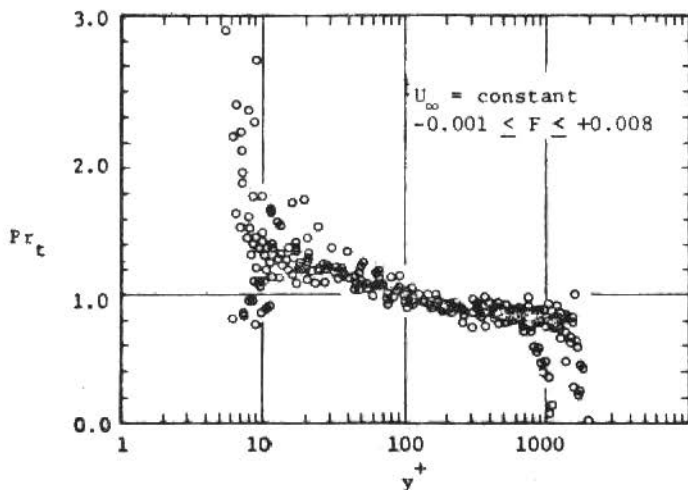
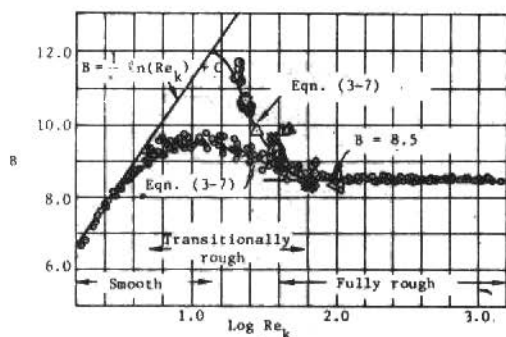


Fig. 47 Turbulent Prandtl number values for smooth, flat-plate flows with suction and blowing (Kays and Moffat, 1975).



10.1	15.8	26.8	39.6	
▽	△			Healzer (1974)
	▲	◆	◀	Pimenta (1975)
⊙ ⁺	x ⁺	• ⁺		Present study

⁺ Artificially thickened
 ⊙ Sandgrain roughness, Nikuradse (1933)

Fig. 48 Variation of B with Re_k for sand-grain roughness and deterministic roughness (spheres) (Ligrani, 1979).

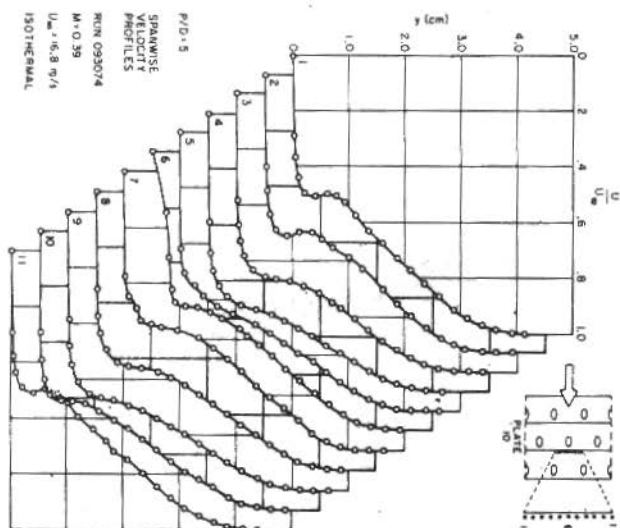


Fig. 49. Velocity profiles at different spanwise locations, 30° slant-angle injection, $M = 0.39$. (Crawford et al., 1976).

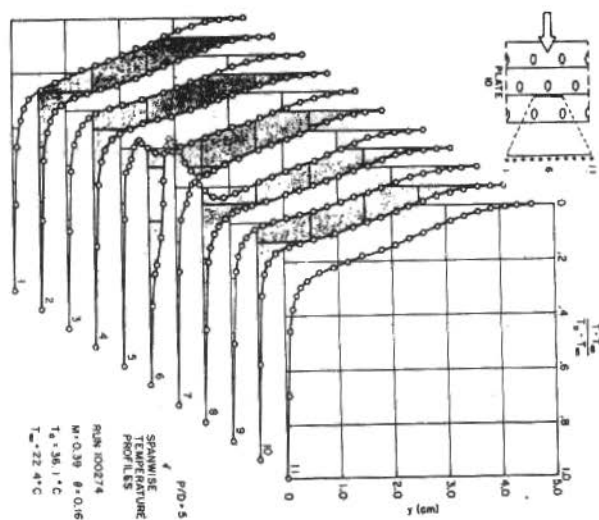


Fig. 50. Temp. profiles at different spanwise locations with full-coverage film cooling, 30° slant-angle injection, $\theta = 0.16$, Crawford, 1976).

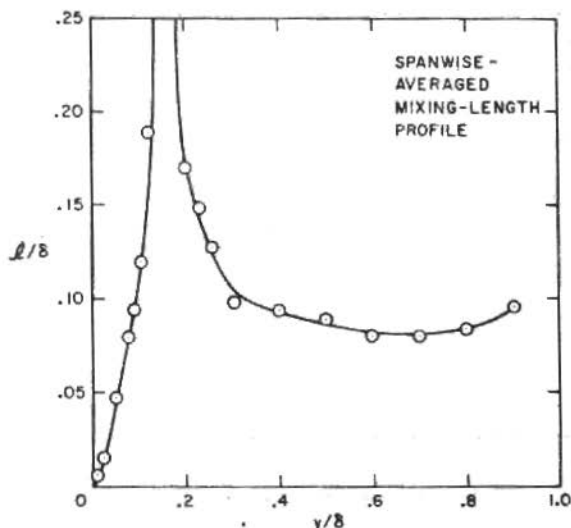


Fig. 51. Mixing lengths deduced from the spanwise average of the velocity profiles, 30° slant-angle, $M = 0.39$ (Crawford et al., 1976).

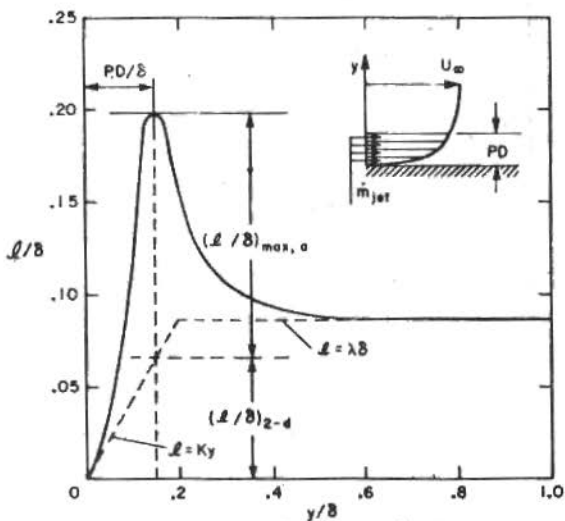


Fig. 52. The mixing-length model for 30° slant-angle injection (Crawford et al., 1976).

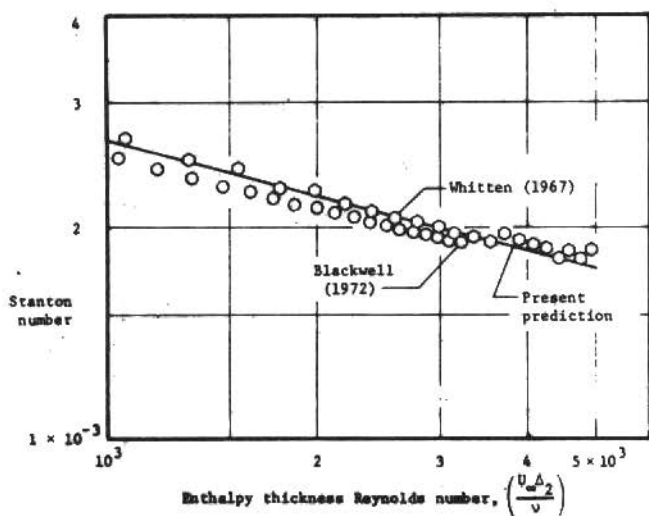


Fig. 53. Comparison of predicted and measured Stanton numbers for flat-plate, constant wall temperature.

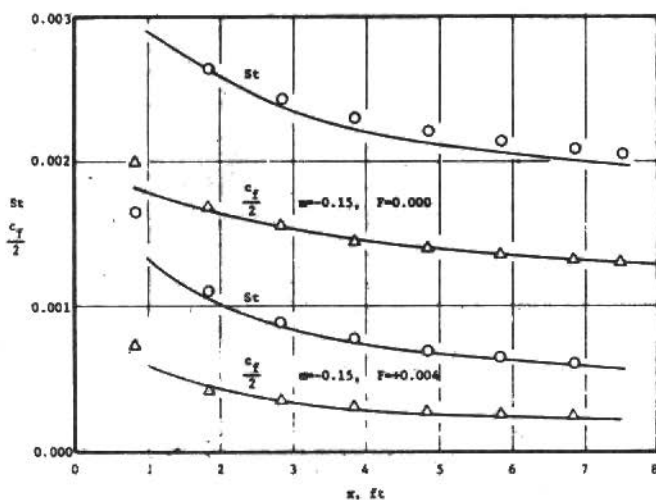


Fig. 54. Comparison of predicted and measured Stanton number and friction factor distributions on a smooth, flat plate with deceleration and blowing.

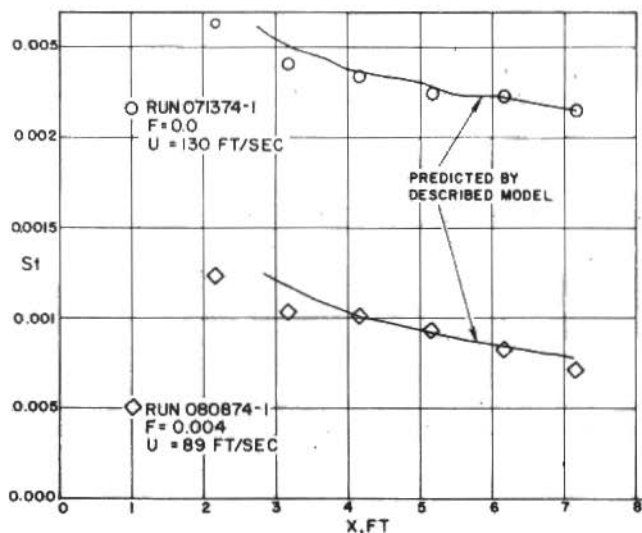


Fig. 55. Comparison of predicted and measured Stanton numbers on a rough surface with and without blowing.

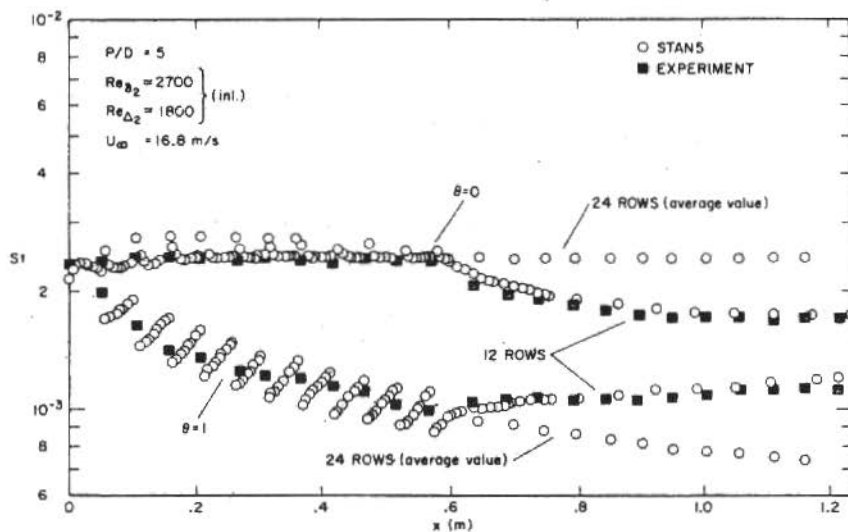


Fig. 56. Comparison of predicted and measured Stanton numbers on a flat surface with discrete-hole injection.

PEDIDO DE ASSINATURA DA RBCM
OU NÚMEROS ATRASADOS QUER DA REVISTA OU ANAIS DE CONGRESSOS

- Preencha a ficha abaixo, indicando o desejado, e remeta para ABCM.

Secretaria da ABCM
PUC/RJ - ITUC
Rua Marquês de São Vicente, 225 - Gávea
22453 - Rio de Janeiro, RJ - Brasil

- Remeta, em anexo, um cheque nominal (Associação Brasileira de Ciências Mecânicas) no valor indicado na referida ficha.

	BRASIL AMÉRICA LATINA	EXTERIOR
Anais do COBEM _____	() 3,0 OTN'S	() US\$ 100,00
Anais do SIBRAT _____	() 2,0 OTN'S	() US\$ 50,00
Anais do ENCIT _____	() 2,0 OTN'S	() US\$ 50,00
Número avulso RBCM _____	() 1,0 OTN'S	() US\$ 15,00
Assinatura da RBCM _____	() 2,0 OTN'S	() US\$ 40,00

ASSINALE SUA SOLICITAÇÃO

NOME _____

ENDEREÇO _____

CIDADE _____ ESTADO _____ CEP _____

